NASA CONTRACTOR REPORT

NASA CR-2429

NASA CR-2429

ANALYSIS OF WING-BODY INTERACTION FLUTTER FOR A PRELIMINARY SPACE SHUTTLE DESIGN

by Richard R. Chipman and Peter Shyprykevich

Prepared by
GRUMMAN AEROSPACE CORPORATION
Bethpage, N.Y. 11714
for Langley Research Center

NATIONAL AERONAUTICS AND SPACE ADMINISTRATION • WASHINGTON, D. C. • JULY 1974

ERRATA

NASA Contractor Report CR-2429

ANALYSIS OF WING-BODY INTERACTION FLUTTER FOR A PRELIMINARY SPACE SHUTTLE DESIGN

By Richard R. Chipman and Peter Shyprykevich

July 1974

Page 26: Table 7 is in error. Replace table 7 with the attached corrected version.

Issued March 1977

TABLE 7.- FLUTTER ANALYSIS RUN NUMBERS

Aerodynamic configuration	Run number				
	Structural configuration				
	A Complete vehicle	B Orbiter with flexibly attached ET & rigidly attached SRB's	C Orbiter with flexibly attached ET	D Orbiter with rigidly attached ET	E Orbiter
1. Wing alone	1A				
2. Wing & refl. of fuselage	2A				
3. Wing & refl. & slender body of fuselage	3A				3E
4. Wing, fuselage & ET refl. & slender body	4A		4C	4D	
5. Wing, fuselage, ET; & SRB refl. only	5A	5B			
6. Complete aero of orbiter, ET & SRB's	6A	6B			
7. Wing aero plus refl. effects of all bodies	7A				
8. Complete aero with vertical separation of SRB's halved	8A				

1. Report No.	2. Government Accession No.	3. Recipient's Catalog No.
NASA CR-2429		

4. Title and Subtitle	5. Report Date
ANALYSIS OF WING-BODY INTERACTION FLUTTER FOR A PRELIMINARY SPACE SHUTTLE DESIGN	July 1974
	6. Performing Organization Code
7. Author(s)	8. Performing Organization Report No.
Richard R. Chipman and Peter Shyprykevich	
9. Performing Organization Name and Address	10. Work Unit No.
Grumman Aerospace Corporation Bethpage, N. Y.	502-32-02-03
	11. Contract or Grant No.
	NAS1-10635-10
12. Sponsoring Agency Name and Address	13. Type of Report and Period Covered
National Aeronautics and Space Administration Washington, D.C. 20546	Contractor Report
	14. Sponsoring Agency Code

15. Supplementary Notes

Final report.

16. Abstract

Subsonic flutter analyses for a preliminary Space Shuttle design were performed to determine the effect of wing-body aerodynamic interaction on the vehicle flutter speed. It was found that the proximity of the large bodies of the Shuttle to the wing reduces critical flutter speed by 11%. Aerodynamic reflection off the bodies is the dominant interaction effect while aerodynamic forces caused by body motion are of secondary importance in most cases.

The analyses employed a doublet-lattice representation of the Space Shuttle, where in the wing and body surfaces were modeled by a lattice of nonplanar lifting surface elements. Axial singularities were introduced to account for body incidence, volume, and camber (slender body) effects. A series of studies on the placement and number of these elements was performed to ensure convergence of the results.

17. Key Words (Suggested by Author(s))	18. Distribution Statement
Wing-Body Interaction Flutter Analysis Preliminary Space Shuttle Design Doublet-Lattice	Unclassified - Unlimited STAR Category 32

19. Security Classif. (of this report)	20. Security Classif. (of this page)	21. No. of Pages	22. Price*
Unclassified	Unclassified	57	$3.75

*For sale by the National Technical Information Service, Springfield, Virginia 22151

ANALYSIS OF WING-BODY INTERACTION FLUTTER FOR A PRELIMINARY SPACE SHUTTLE DESIGN

by

Richard R. Chipman and Peter Shyprykevich
Grumman Aerospace Corporation, Bethpage, N. Y.

SUMMARY

Subsonic flutter analyses for a preliminary Space Shuttle design were performed to determine the effect of wing-body aerodynamic interaction on the vehicle flutter speed. It was found that the proximity of the large bodies of the Shuttle to the wing reduces critical flutter speed by 11%. Aerodynamic reflection off the bodies is the dominant interaction effect while aerodynamic forces caused by body motion are of secondary importance in most cases.

The analyses employed a doublet-lattice representation of the Space Shuttle, wherein the wing and body surfaces were modeled by a lattice of nonplanar lifting surface elements. Axial singularities were introduced to account for body incidence, volume, and camber (slender body) effects. A series of studies on the placement and number of these elements was performed to ensure convergence of the results.

INTRODUCTION

The flutter characteristics of an aircraft component can be affected by aerodynamic interaction between it and other proximate components. Classic examples, when both components are lifting surfaces, are T-tail flutter (ref. 1) and wing-tail flutter (ref. 2). To predict subsonic aerodynamic forces arising in such configurations, the kernel function method of Watkins (ref. 3) and the doublet-lattice method of Rodden (ref. 4) and of Stark (ref. 5) were developed and extended to handle multiple planar and nonplanar surfaces. The success obtained in applying

these theories to wing-tail configurations is recorded by Sensburg (ref. 6), Mykytow (ref. 7), and Triplett (ref. 8). Similarly, Chipman used the doublet-lattice flutter analyses method to correlate successfully with wind tunnel data for pairs of closely spaced wings such as might be found on the fly-back-booster Space Shuttle configurations (ref. 9).

The calculation of aerodynamic forces arising from the interaction between bodies and lifting surfaces is fairly recent. Woodward (ref. 10) developed a method for steady flow which determines aerodynamic influence coefficients for such configurations. Similar work has been performed by Hess (ref. 11). By extending the Woodward method to quasi-steady flow, Huntington (ref. 12) has shown that wing-body interaction effects can be substantial on vehicle gust-response characteristics.

For unsteady flow, Rodden and Giesing (ref. 13) developed a technique which combines the doublet-lattice method with Miles' slender body theory (ref. 14). Additionally, Giesing (ref. 15) has added the method of images to this technique.

The present Space Shuttle concept features four large, flexible bodies: the orbiter fuselage, the external tank (ET), and the two solid-rocket boosters (SRB's). The proximity of these bodies to the orbiter wing admits the possibility of a change in vehicle flutter boundary as a result of aerodynamic interaction. Consequently, a two-phase study has been initiated to obtain analytical and experimental confirmation of this contention. This report summarizes the first phase of this work: A preliminary design – the Grumman G III – of the parallel-burn, Space Shuttle concept is analyzed using Rodden's method (ref. 13) to determine the effect of wing-body aerodynamic interaction on flutter.

SYMBOLS

$[A_B]$ slender-body aerodynamic operator

c_{p_j} nondimensional pressure for jth mode

$\left[D_w\right]$	aerodynamic operator for wing alone
$\left[D_{w,I}\right]$	aerodynamic operator for wing and interaction panels
ET	external tank
$\left[F_B\right]$	slender-body downwash operator
M	Mach number
$Q_{R,S}$	nondimensional generalized forces for Rth pressure mode and Sth deflection mode
SRB	solid-rocket boosters
V-g-f	velocity-damping-frequency
w_j	downwash for jth mode
$\left\{w_W\right\}$	wing downwash distribution
$\left\{w_B\right\}$	body downwash distribution
$\left\{w_{W,B}\right\}$	wing downwash distribution due to body
$\left\{w_{B,B}\right\}$	body downwash distribution on interaction panels due to body
x	axial dimension
y	spanwise dimension
z	vertical dimension
$\left\{\Delta C_{p(i)}\right\}$	nondimensional pressure distribution for the ith pressure type

THEORY

Vibration Analysis

Before performing flutter studies, vibration characteristics of the Grumman version of the Space Shuttle (figure 1) were determined. The flight trajectory point chosen for the study was at M = 0.8 and an altitude of 4,570 m (15,000 ft). The weight distribution appropriate to this point was used and summarized by component weights in table 1.

The vibration analysis was performed using standard matrix methods. The flexibility data for the orbiter were obtained from a large finite element model. The one full-span control surface was considered rigid although attached flexibly to the wing. These data were subsequently reduced and force-coupled through the attachment points to the beam idealizations of the external tank and the SRB's. These couplings were all statically determinate. Table 2 summarizes the interstage flexibilities (including the local structure around the attachment points). The symmetric vibration analyses employed 120 degrees of freedom, and the antisymmetric vibration analyses consisted of 145 degrees of freedom.

Vibration analyses were performed for the complete vehicle, for the orbiter and external tank without SRB's, and for the orbiter alone. Various interstage coupling flexibilities were also investigated. The attachment between the external tank and the SRB's is quite flexible, so that a large stiffness range is covered by the rigid and actual attachments.

Tables 3 and 4 summarize the results of the vibration analysis. Frequencies and dominant component motion are identified for both symmetric and antisymmetric conditions. Mode shapes for the complete vehicle are presented in figure 2; only the modes which are important for flutter are shown. Symmetrical modes are indicated by the vertical motions of the orbiter and external tank, vertical and lateral motions of the SRB, and fore-and-aft motion of the fin. Antisymmetrical

modes are shown by the vertical motions of the wing, lateral motions of the fuselage, fin, and external tank, and vertical and lateral motions of the SRB. The rotational degrees of freedom (not shown in figure 2) were included in the analysis. For completeness, the generalized mass are included in table 5.

Aerodynamic Analysis

Subsonic generalized aerodynamic forces were calculated for the configurations studied by direct application of the nonplanar doublet-lattice method of ref. 13. In this method lifting surfaces are modeled by a lattice of doublet panels. The effects of isolated bodies are represented by axial doublets whose strengths are independently determined by slender body theory. Interaction between bodies and lifting surfaces is obtained by placing doublet panels on the idealized surface of each body in regions close to the lifting surfaces.

The strength of the doublets on the body and lifting surfaces are calculated simultaneously to produce normalwash on their boundaries. The slender body and surface panel solutions are coupled by assuming that the axial doublets from the slender body solution affect the boundary conditons that must be satisfied by the surface doublets. Thus, before the strengths of the surface panel doublets are determined, the normalwash prescribed on the wings and interaction regions is decremented by the normalwash generated on these surfaces by the axial doublets. For single-body configurations, this subtraction results in a zero body-netwash, since the slender body solution already satisfies the prescribed wash on the body surface. For more than one body, the body panel netwash is no longer equal to zero due to small contributions of normalwash caused by the axial elements of other bodies.

This method may be better understood by considering a single wing and body pair. The generalized aerodynamic forces are produced by the contribution of six distinct types of pressure distributions. The vibration of the wing causes three of these pressures:

1. A direct pressure on the wing itself
2. A direct pressure on the body
3. A pressure on the wing due to reflections off the body

Similarly, the remaining three pressure distributions arise from the vibration of the body

4. A direct pressure on the body itself
5. A direct pressure on the wing
6. A pressure on the body due to reflections off the wing.

These effects are illustrated in figure 3.

In the doublet-lattice method, these pressures are computed using the aforementioned lifting surface panels, slender body elements, and interaction panels. Specifically, the vibration of the wing produces a downwash which, if the wing is alone, gives rise to pressure no. 1:

$$\left\{w_W\right\} = \left[D_w\right] \left\{\Delta C_{p(1)}\right\} \tag{1}$$

When a set of rigid interaction panels are placed in proximity with the wing, pressure nos. 2 and 3 are produced:

$$\begin{Bmatrix} w_W \\ o \end{Bmatrix} = \begin{bmatrix} D_{w,I} \end{bmatrix} \begin{Bmatrix} \Delta C_{p(1)} + \Delta C_{p(3)} \\ \Delta C_{p(2)} \end{Bmatrix} \tag{2}$$

Using slender body theory, pressure no. 4 is determined directly from the downwash, $\left\{w_B\right\}$, generated by the motion of the body:

$$\left\{\Delta C_{p(4)}\right\} = \left[A_B\right] \left\{w_B\right\} \tag{3}$$

The axial singularities to generate this pressure augment the downwash field over that due to the motion of the lifting surface and reflecting panels:

$$\begin{Bmatrix} w_{W,\,B} \\ w_{B,\,B} \end{Bmatrix} = \begin{bmatrix} F_B \end{bmatrix} \begin{Bmatrix} \Delta C_{P(4)} \end{Bmatrix} \tag{4}$$

This, in turn, gives rise to the final two pressures:

$$\begin{bmatrix} D_{w,I} \end{bmatrix} \begin{Bmatrix} \Delta C_{p(1)} + \Delta C_{p(3)} + \Delta C_{p(5)} \\ \Delta C_{p(2)} + \Delta C_{p(6)} \end{Bmatrix} = \begin{Bmatrix} w_W - w_{W,B} \\ w_B - w_{B,\,B} \end{Bmatrix}$$

$$= \begin{Bmatrix} w_W - w_{W,B} \\ 0 \end{Bmatrix} \tag{5}$$

The generalized forces for the wing and body pair are then obtained from the products of the ΔC_p's from eq. (3) and (5) and their corresponding mode shapes.

For configurations with more surfaces and bodies than the wing and body pair, equations similar to eq. (1) through (5) are solved. However, due to the complexity of notation, they are not included here.

Aerodynamic Idealization

As seen from figure 1, the Space Shuttle is comprised of five main components: the wings, the fin, the orbiter fuselage, the external hydrogen-oxygen tank (ET), and two solid-rocket boosters (SRB's). For purposes of this study, consideration of the fin is omitted. Figures 4A and 4B show the aerodynamic element combination used to model this configuration. The wing is modeled by a lattice of doublet panels. The fuselage and the external tank are each represented by a line of axial doublet elements whose orientations are vertical in the symmetric case and horizontal in the antisymmetric case. Similarly, the SRB's are modeled by axial doublets but, since the

SRB's are located off the vehicle midplane requiring both lateral and vertical degrees of freedom in both the symmetric and antisymmetric cases, each SRB must be represented by two sets of axial doublets, one oriented horizontally and one oriented vertically.

To account for interaction between the bodies and the wing, doublets are applied to the idealized surfaces of each body in the regions close to the wing.

Vehicle Idealization Studies

Before deciding upon the idealization to be used in the flutter analysis, variations in number and distribution of aerodynamic elements were studied to determine their effect on generalized forces and flutter speed. In all, variations in the following parameters were made:

- Chordwise and spanwise number of wing lattice boxes
- Circumferential distribution of orbiter fuselage interaction panels
- Axial distribution of fuselage panels
- Number and location of slender body elements for the orbiter fuselage.

Wing lattice boxes - Seven different combinations of lattice boxes were used to idealize the wing planform. Flutter analyses of the isolated wing with as few as 28 boxes (7 chordwise and 4 spanwise) and as many as 88 boxes (11 chordwise and 8 spanwise) were run. Less than one percent variation in flutter speed was obtained, indicating that accurate results can be obtained with rather coarse paneling.

Interaction panels - The cross-section of the fuselage was modeled seven different ways, as shown in figure 5. Assuming that the seventh case represents the converged solution, comparisons are made for other models using case 7 as a base. Table 6 contains the generalized force comparison for the above cases. The generalized forces were computed for the symmetric modes of the "orbiter alone" configuration and are

shown for the first two modes only. As can be seen, even a crude model (1 or 2) gives reasonable accuracy. Model 5 was subsequently used for final flutter analyses.

A limited number of variations in the number and axial locations of fuselage panels were considered. The recommendations of ref. 13 were followed to the extent that panel edges coincided with wing root panel edges. Generalized forces for dense and sparse paneling, as shown in figure 6, are compared in table 6. The differences are very small, indicating that the solution is not sensitive to the number of longitudinal panels. It should be noted that, even for the large grid, the panel length is within the recommended limits, i.e., the box length is small compared to the basic wavelength.

In modeling bodies that are in close proximity, convergent results were obtained only if the axial panel edges coincided. This is the reason for the longitudinal compatibility of the boxes on the orbiter fuselage, the external tank and the SRB's. To improve numerical resolution much care was exercised in modeling the complete vehicle, aligning spanwise and chordwise panel edges as much as possible. For instance, three additional strips of wing panels were added to align wing panel spanwise edges with the SRB panels. This edge alignment produced convergent results with the least number of panels.

Slender body elements - Slender-body-element definitions of the orbiter fuselage were varied to determine the resulting pressures' sensitivity to the number and location of such elements. Three different representations, shown in figure 7, were analyzed. The real part of pressures calculated for two fuselage-bending modes are plotted together with the corresponding mode shapes. As can be seen, the number and location of elements is not very critical, although the density of panels should be higher at body radius changes and for higher-order modes. The densest element distribution was used in the flutter analyses.

In summary, the experience gained in using the doublet-lattice program has shown that the recommendations of ref. 13 are good guidelines but that, in complex configurations, various models should be tried to ensure convergence of the generalized aerodynamic forces. With proper panel alignment, however, an adequate solution can be obtained with a relatively sparse grid.

PARAMETER STUDY DESCRIPTION

Aerodynamic Variations

To isolate the effects of each component in the aerodynamic idealization on the flutter speed of the vehicle, a series of analyses were made using a single set of vibration modes but varying the aerodynamic composition of the configuration. The modes used were those of the complete shuttle, shown in figure 2. Results of these analyses were compared with those of a base configuration consisting of aerodynamic forces from the orbiter wing along -- without any reflections off the bodies.

In table 7, the configurations studied are denoted. Run 1A, the base case, has only pressures of type no. 1, as in eq. (1). Run 2A includes interaction panels on the orbiter fuselage, but does not include axial elements. Consequently by comparing 2A with the base, 1A, the effects of reflection off the orbiter body are isolated (pressure type no. 3, as in eq. (2)). Axial elements modeling the fuselage are included in run 3A, so that all pressure types no. 1-6 are present as in eq. (5). In 4A, interaction paneling and axial elements are placed on the external tank. Similarly, 5A includes interaction panels on the SRB and 6A includes axial elements for the SRB. Configuration 7A has interaction panels on the surface of all bodies but no axial elements. Since 6A includes axial elements and interaction panels on all bodies, it is the most complete representation studied.

An additional run, 8A, was run using a complete aerodynamic representation as in run 6A but with the separation between the SRB and the wing halved.

Structural and Configurational Variations

In addition to variations in aerodynamic idealization, various combinations of components and structural idealizations of the Space Shuttle were also analyzed for flutter. The configurations studied are summarized in table 7 as different columns (letter series). Since each row of this table denotes the same aerodynamic configuration, comparison across columns provides correlation between different component combinations and structural idealizations. Thus, column A represents the complete Space Shuttle structure: free-free flexible orbiter, flexibly connected flexible external tank with flexibly attached flexible SRB's. All other configurations are simplifications of the above configuration and are, in a way, a measure of how much the configuration or structure can be simplified without sacrificing accuracy in computing vehicle flutter speed.

RESULTS OF ANALYSIS

Flutter Modes for Base Configuration

Figures 8 and 9 show the V-g-f plots for the base configuration (run 1A) in the symmetrical and antisymmetrical cases, respectively. The antisymmetric flutter speed is lower and, therefore, is the critical flutter speed. Tables 8 and 9 present the major modal contributions to the eigenvectors of the various flutter instabilities. The roots are numbered in ascending frequency order. In the symmetric case the principal flutter instabilities are as follows:

- The lowly damped 7th root instability. This root is primarily the seventh mode, first fuselage bending causing wing plunge or heave. This couples with the fourth and fifth modes, which are both first wing-bending-type modes, creating a slight instability at speeds as low as 221 m/sec (430 knots). If a damping level of 0.01 is chosen as representative of the actual structural damping, the root does not go unstable.
- The 9th root instability at 365 m/sec (710 knots) for 0.01 damping. The main contributor to this root is the ninth mode, which is a fuselage bending mode causing wing pitch. It is strongly unstable when aerodynamically coupled with the fourth and fifth modes. Coupling with the eleventh mode also is present.

- The 11th root instability at 388 m/sec (755 knots) for 0.01 damping. This root is made up almost equally of modes 10 and 11 approximately 180^{o} out of phase. It also is strongly unstable. Coupling with the sixteenth, fourth, fifth, seventeenth, and ninth modes is important.

If all modes except those mentioned above are eliminated from the analysis the flutter characteristics are virtually unchanged, as shown in figure 10.

For the antisymmetric case there are five principal instabilities:

- The 9th root instability at 303 m/sec (590 knots) for 0.01 damping. The ninth mode, wing first torsion, couples with the sixth through eight modes (wing bending modes) and the tenth mode.
- The 10th root instability at 290 m/sec (565 knots) for 0.01 damping. The main contributor is the tenth mode, which is a fuselage bending mode causing wing pitch. It couples with the sixth through ninth modes .
- The 12th and 13th root instabilities at 344 and 336 m/sec (670 and 650 knots) for 0.01 damping. Both of these roots are comprised mainly of the twelfth mode, which is third fuselage bending causing wing pitch. This couples aerodynamically with modes six, eight, and ten. Wing heave modes thirteen and fifteen contribute to the first and second of these instabilities, respectively.
- The 11th root instability at 496 m/sec (965 knots) for 0.01 damping. The eleventh mode is a fuselage bending causing wing pitch (much like the tenth mode) and couples with modes eight and ten.

If only modes 6 through 15 are retained in the analysis, all instabilities except the 11th root are predicted with fair accuracy, as shown in figure 11.

Effects of Aerodynamic Interaction - Antisymmetric

Table 10 shows the flutter speeds and flutter speed ratios obtained for the various roots in each of the antisymmetric analyses, while table 8 and 9 present the modal composition of the flutter vectors. To determine distinct flutter speeds to facilitate comparisons for lowly damped instabilities a structural damping level of 1% is assumed, as was done in the base case. Roots nine and ten are highly coupled in all configurations so that uniqueness is difficult to obtain; consequently, the damping

characteristics of these roots seem to interchange from configurations 1A and 2A to 3A through 6A. To make appropriate comparisons between runs, the more unstable of these two roots is referred to as root ten while the less unstable is denoted root nine. For example, in the V-g-f plot for run 6A (figure 12), the root-ten flutter speed ratio is calculated using the ninth (lowest) root since it is more unstable than the tenth.

In examing table 10, first consideration is given to root ten since it has the lowest flutter speed. Body aerodynamics (body motion plus body interaction) lowers this flutter speed by 11%. Of this reduction, 6% is attributed to the presence of the orbiter (run 3A), 1% to the external tank (run 4A), and 4% to the SRB's (6A). If the slender-body aerodynamics were neglected, the reduction would be 8% (run 7A); consequently, body motion (in an aerodynamic sense) is not too important to this mechanism.

Root nine, which was only marginally unstable in the base case, is destabilized 13% by simple reflection off the rigid bodies (run 7A), but is stable when body motion is included in the analysis as in runs 3A-6A.

The flutter speeds of roots twelve and thirteen are lowered only 6% by body aerodynamic effects, about half the effect being caused by body motion and half by reflection.

Much like root ten, root eleven experiences an 8% reduction in flutter speed due to simple reflection. Body motion (of the fuselage), however, has a pronounced effect on this mechanism, lowering the flutter speed an additional 22%. This reduction is accompanied by a drastic change in the phasing of the flutter vector components. Computing phase angles from the real and imaginary parts of the eigenvectors presented in table 9, one finds that in the base run modes 8 and 10 lead mode 11 by 49^{o} and 74^{o}, respectively, but lag mode 11 by 8^{o} and 172^{o} in run 6A.

To determine the relative importance of the body aerodynamic forces which cause these changes in flutter speed, inspection is made of the generalized aero-

dynamic force matrix for a reduced frequency near flutter. Table 11 shows selected elements of this matrix for runs 1A, 6A, and 7A. In particular, the elements selected are those involving the major modal contributors to roots ten and eleven. For each element, this table has three columns which correspond respectively to the summation of forces caused by pressures on the wing panels alone, on the wing and interaction panels, and on the total vehicle, i.e., the wing and interaction panels and the axial elements.

Referring to eq. (1), one sees that the base run consists of only pressure type no. 1 of page 6 . As eq. (2) indicates, pressure types no. 1 and 3 appear on the wing in run 7A. For run 6A, eq. (5) illustrates that the generalized forces of column one in table 11 arise from pressure no. 1, 3, and 5, while those of column two include effects of pressure no. 2 and 6 and those of column three also include pressures of type no. 4.

By comparing the various table entries, one can assess the relative importance of a particular body aerodynamic effect on the generalized forces. For example, comparison of the $Q_{11,S}$ and $Q_{R,11}$ terms indicates that reflection effects are not as important to this force as slender body effects and that pressure of type no. 4 is particularly large in this case.

If, for instability 10, attention is confined to the principal modes involved (8, 9, and 10) and table 11 is consulted, the following simplified explanation of the effect of body aerodynamics emerges. Mode 8, the driving mode of the flutter mechanism, is wing bending almost exclusively (disregarding fin motion) and, as such, contributes little or no body-motion forces. Only reflection of signals from the wing affects the mode-generated aerodynamic forces. Mode 9, wing torsion, also has a small amount of body motion; again, reflection off the bodies is the only substantial interaction effect. Mode 9 is affected more than mode 8 because torsion involves more motion inboard (close to the reflecting bodies) than does bending. Mode 10, structurally coupling fuselage bending and wing pitch, has significant body motion which

generates aerodynamic forces (type no. 4-6) and has considerable wing root motion which makes reflection (type no. 3) important. From this detailed account, we see that reflection is the major factor affecting the root 10 instability, although body motion is of some significance.

For root 11, modes 8, 10, and 11 are principal modes. Mode 11 is similar to 10 in that reflection and body-motion effects are both important but, in mode 11, the latter is the more important of the two. Since the root 11 instability involves two modes (10 and 11) where body motion is important, a larger variation in flutter speed due to body-motion (22%) is experienced for this coupling mechanism.

As an additional indication of how important body motion is to the flow field, figure 13 shows the effect on the wing of the downwash induced by body motion for mode 11. Corresponding to the right-hand side of eq. (5), the augmented downwash is quite different from the prescribed downwash. Figure 14 shows the resulting differences in wing pressures.

Effects of Aerodynamic Interaction - Symmetric

Table 10 gives the flutter speeds of the various roots in the symmetric analyses, while table 8 presents the flutter vector composition for runs 1A and 6A. Figure 15 shows the V-g-f plot for run 6A.

In examining root 9, the principal instability, body aerodynamics is seen to lower the flutter speed by 9%, of which 3% is attributed to the presence of the orbiter, 2% to the external tank, and 4% to the SRB's. If the aerodynamics due to body motion were neglected, run 7A indicates that the reduction would be 6%. As in the antisymmetric case, body reflection associated with wing motion has a greater effect than body motion on the flutter speed of the principal instability.

The flutter speed of root 11 experiences a mere 2% reduction due to body aerodynamics, and this is seen to result from SRB reflection effects. The marginally stable 7th root first becomes unstable (.01 damping level) for configuration 3A at

288 m/sec (560 knots) with the introduction of fuselage motion. It becomes more stable by reflection of other bodies and removal of fuselage motion (run 7A). The external tank motion also tends to stabilize this marginally unstable root (run 4A).

As in the antisymmetric runs, an examination of the generalized aerodynamic force matrix for a reduced frequency near flutter is made. Table 12 shows the elements of this matrix that relate to major modal contributors of root 9 for runs 1A, 6A, and 7A. The body aerodynamic effects can be understood in the following way. Since mode 4 has little body motion, only reflection can have a big effect on its generalized forces. As a bending mode, however, mode 4 has little wing motion at its root (close to the reflecting bodies) and, hence, is affected little by interaction Mode 5, also a wing bending mode, has some body motion, causing changes in the aerodynamic forces. As a fuselage-bending/wing-pitch mode, mode 9 has both considerable reflection and body motion effects. Like mode 4, mode 11 has little body motion, and body effects are limited to reflection. With this composition, the response of root 9 to reflection effects and relative insensitivity to body motion is easily comprehended.

Effects of SRB Proximity

As shown in table 10, halving the separation between the top of the SRB and the wing does not significantly affect flutter speed. To investigate this phenomenom, generalized forces in the antisymmetric case were calculated at a reduced frequency near flutter for various separations, giving the trends of figure 16. As shown, reflection effects level out at a separation of about one-half the SRB radius. Any increased proximity past this point has almost no effect. Since the present analysis uses linear aerodynamic theory and does not account for the Venturi effects that would arise when the SRB is close to the wing, this conclusion is of doubtful validity.

Structural and Configurational Effects

To obtain the mass and structural effects of the external tank and SRB's upon the vehicle flutter speed, several additional analyses were performed, as indicated in table 7, and compared with the A-series of runs which use the modes of the complete vehicle. For each set of comparisons, the same aerodynamic idealization was used. Table 13 summarizes the results.

The omission of the SRB's results in a 3% and 8% decrease in the critical flutter speed (comparison of runs 4C and 4A) for the symmetric and antisymmetric conditions, respectively. Since the flutter mechanism involves essentially the same type of modes, the different flutter speed can be attributed to small changes in frequencies, mode shapes, and phasing.

While the omission of the external tank and the SRB's (3A vs 3E) does not change the flutter speed for the antisymmetric case, there is a 5% drop for the symmetric case. Again, the flutter mechanisms are essentially identical. Ignoring tank aerodynamic effects, flutter calculations for the orbiter alone are conservative.

Studies were also made of the effect of interstage flexibilities on flutter. For the symmetric case, making the interstage connection rigid between the external tank and the orbiter decreases the flutter speed by 8% (comparison of runs 4C and 4D). The drop in flutter speed is traced to a change in the flutter mechanism; viz, a coalescence involving a mode in closer proximity to the driving mode. Mode 3 (originally at 2.97 cps) is now flutter-critical as opposed to mode 4 at 3.32 cps. Both modes are fuselage and external tank bending with wing pitch. In the symmetric case, a 5% drop in flutter speed occurs.

The interstage connection between the external tank and the SRB seems to have little effect on flutter speed. This is shown by comparing runs 5A, 6A representing a soft connection with runs 5B, 6B in which the connection is rigid. Only a 2% change is realized. The small difference is attributed to the fact that SRB mode and fre-

quency changes have little effect on the flutter mechanism which, throughout the whole study, has been consistently wing bending-fuselage bending/wing pitch. The results indicated here are only applicable to the configuration studied and may not hold for smaller SRB mass.

CONCLUSION

Analytical flutter studies were conducted to determine the effect of wing-body interaction on the flutter speed of a preliminary shuttle design. The Space Shuttle model used included wing and body aerodynamics from the orbiter fuselage, external tank, and SRB's. Studies verified the validity of the guidelines cited in ref. 13 for establishing an appropriate aerodynamic idealization. A converged solution was obtained using 208 lifting surface elements and 63 axial elements.

For the shuttle configuration studied, the critical flutter mechanism was the coupling of the wing-first bending mode with a fuselage-bending/wing-pitch mode. Body aerodynamics reduced the flutter speed corresponding to this mechanism by 11%, with reflection off the bodies being the predominant effect. Body-motion aerodynamics was of secondary importance for this mechanism, but it did have large effects on certain other noncritical flutter modes.

Configurational and structural effects of the external tank and the solid-rocket booster on flutter speed were also evaluated. Whereas excluding aerodynamic coupling from the analysis raised the predicted flutter speed, excluding structural coupling between components reduced the predicted flutter speed. Consequently, an analysis using full vehicle-coupled modes without aerodynamic coupling between components is less conservative than a component analysis. However, both give higher flutter speeds than an analysis including aerodynamic coupling.

Two other parameters studied were SRB vertical location and interstage flexibilities. Decreasing the nominal (half-SRB-radius) separation between the wing and the SRB had no effect on flutter speed, while removing the SRB entirely raised the speed by 4%. Due to the limitations of linear potential theory, the validity of the results for small separations is in doubt. The flexibility of interstage connections between the external tank and the orbiter does affect the flutter speed, however, since the SRB's modes have little effect on flutter, the interstage flexibility between SRB's and the external tank is not an important parameter for the configuration studied.

REFERENCES

1. Stahle, C. V.: Transonic Effects on T-tail Flutter. The Martin Company RM-24, 1959, Baltimore, Md.

2. Topp, L. J.; Rowe, W. S.; and Shattuck, A. W.: Aeroelastic Considerations in the Design of Variable Sweep Airplanes. ICAS Paper No. 66-12, Sept. 1966.

3. Watkins, C. E.; Runyan, H. L.; and Cunningham, H. J.: A Systematic Kernel Function Procedure for Determining Aerodynamic Forces on Oscillating or Steady Finite Wings at Subsonic Speeds. NASA TR R-48, 1959.

4. Albano, E.; and Rodden, W. P.: A Doublet Lattice Method for Calculating Lift Distributions on Oscillating Surfaces in Subsonic Flow. AIAA Journal, Vol. 7, No. 2, Feb. 1969, pp 279-285.

5. Stark, V. J. E.: Aerodynamic Forces on a Combination of a Wing and a Fin Oscillating in Subsonic Flow SAAB TN 54, Feb. 1964, Linkoping, Sweden.

6. Sensberg, O.; and Laschka, B.: Flutter Induced by Aerodynamic Interference between Wing and Tail. Journal of Aircraft, Vol. 7, No. 4, July-Aug. 1970, p. 319-324.

7. Mykytow, W. J.; Noll, T. E.; Huttsell, L. J; and Shirk, M. H.: Investigations Concerning the Coupled Wing-Fuselage-Tail Flutter Phenomenon. Journal of Aircraft, Vol. 9, No. 1, Jan. 1972, p. 48-54.

8. Triplett, W. E.; Burkhart, T. H.; and Birchfield, E. B.: A Comparison of Methods for the Analysis of Wing-Tail Interaction Flutter. AIAA Paper 70-80, presented at Aerospace Sciences Meeting, Jan. 19-21, 1970, N.Y., N.Y.

9. Chipman, R. R.; Rauch, F. J.; and Hess, R. W.: Flutter of Pairs of Aerodynamically Interfering Delta Wings. Journal of Aircraft, Vol. 5, No. 6, pp. 728-734, Dec. 1973.

10. Woodward, F. A.: Analysis and Design of Wing-Body Configurations at Subsonic and Supersonic Speeds, Journal of Aircraft, Vol. 5, No. 6, pp. 528-534, Dec. 1968.

11. Hess, J. L. and Smith, A. M. O.: Calculation of Non-Lifting Potential Flow about Arbitrary Three Dimensional Bodies. Douglas Aircraft Company Report No. E.S. 40622, 1962.

12. Huntington, R. G.: Space Shuttle Response to Atmospheric Turbulence. AIAA Paper 73-310 presented at the AIAA Dynamics Specialists Conference, Williamsburg, Virginia, March 1973.

13. Rodden, W. P.; Giesing, J. P., and Kalman, T. P.: New Developments and Applications of the Subsonic Doublet-Lattice Method for Nonplanar Configurations, AGARD Symposium on Unsteady Aerodynamics for Aeroelastic Analyses of Interfering Surfaces, Paper No. 4, presented in Tonsberg, Oslofjorden, Norway, November 1970, AGARD-CP-80-71.

14. Miles, J. W.: On Non-Steady Motion of Slender Bodies Aeronautical Quarterly, Vol. II, Nov. 1950, pp. 183-194.

15. Giesing, J. P.; Kalman, T. P.; and Rodden, W. P.: Subsonic Unsteady Aerodynamics for General Configurations. AIAA Paper 72-26 presented at the 10th AIAA Aerospace Sciences Meeting, San Diego, California, Jan. 1972.

TABLE 1. – TOTAL WEIGHTS OF SPACE SHUTTLE

Component	Mass, kg	Weight, lb
Orbiter	153,044	337,405
ET	726,383	1,601,401
SRB (2)	1,041,645	2,296,435
Total	1,921,072	4,235,241

TABLE 2. – LOCAL INTERSTAGE FLEXIBILITIES

Local attachment		Symmetric flexibilities		Antisymmetric flexibilities	
		m/N x 10^8	(in./lb x 10^6)	m/N x 10^8	(in./lb x 10^6)
SRB/ET[a] fwd	x	0.782	(1.37)	0.782	(1.37)
	y	3.809	(6.67)	10.706	(18.75)
	z	7.040	(12.33)	5.710	(10.00)
SRB/ET[a] aft	y	3.809	(6.67)	10.706	(18.75)
	z	7.040	(12.33)	5.710	(10.00)
Orbiter/ET[b] fwd	y	–	–	1.456	(2.55)
	z	4.796	(8.40)	–	–
Orbiter/ET[b] aft	x	1.612	(2.82)	–	–
	z	.910	(1.59)	–	–
	x-z[c]	-.0296	(-.0519)	–	–
	y	–	–	1.753	(3.07)
	θ_x	–	–	.000105	(.000184)
	y-θ_x[c]	–	–	-.00628	(-.011)

[a] Flexibility is from ℄ of SRB to ℄ of ET.

[b] Flexibility is from orbiter attachment point to ℄ of ET.

[c] Off-diagonal (coupling) terms

TABLE 3. – NATURAL FREQUENCY AND MODE INDEX SUMMARY, SYMMETRIC MODES

Mode	Natural frequency, Hz and (mode index)				
	Structural configuration				
	A Complete vehicle	B Orbiter with flex. attached ET & rigid. attached SRBs	C Orbiter with flex. attached ET	D Orbiter with rigid. attached ET	E Orbiter
ET bending, orbiter pitch	(1) 1.30	(1) 1.42	(1) 1.46	(1) 1.62	
SRB lateral bending	(2) 1.39	(2) 2.80			
SRB vertical pitch, orbiter transl	(3) 1.62				
1st wing bending	(4) 2.02	(3) 2.07	(2) 2.12	(2) 2.14	(1) 2.20
Fuselage, ET bending; wing bending/torsion, SRB yaw	(5) 2.36 (6) 2.53	(4) 2.42	(3) 2.56		
Fuselage, ET bending; wing bending/torsion, SRB pitch		(5) 2.56			
Fuselage, ET bending; wing torsion /heave	(7) 2.64			(3) 2.97	
ET bending; fuselage, wing pitch	(8) 2.75				
Fuselage, ET bending out of phase; wing pitch	(9) 3.40		(4) 3.32	(4) 3.41	
Fuselage, ET bending in phase; wing pitch		(6) 3.40	(5) 3.67/4.27	(5) 3.80	(2) 3.23
Fuselage, ET bending, SRB v. bending, wing transl		(7) 3.60			
Fuselage ET bending out of phase, wing transl	(10) 4.16	(8) 4.03			
Wing bending, RCS[a] pitch	(11) 4.54	(9) 4.55	(6) 4.56	(6) 4.53	(3) 4.54
Fuselage, ET bending, wing pitch/torsion	(12) 4.64				
Fuselage, SRB bending, wing torsion/transl		(10) 4.93	(7) 4.97		
Fuselage, SRB bending, wing torsion/transl	(13) 5.31	(11) 5.08			
Fuselage 2nd bend. ET 3rd bend.; wing roll, pitch				(7) 5.68	
Fuselage 3rd bending, wing torsion	(14) 5.83			(8) 5.87	
SRB vertical & lateral bending	(15) 5.98				
Fuselage 3rd bending, wing roll					(4) 6.16
Fuselage 3rd bending, wing bending/roll	(16) 6.26	(12) 6.26	(8) 6.26	(9) 6.41	(5) 6.40
Fuselage 2nd bend ET 3rd bend.; wing roll	(17) 7.37	(13) 6.65	(9) 7.16		
Fuselage 3rd bend ET 3rd bend.; wing pitch/roll		(14) 7.75		(10) 7.92	
Fuselage 3rd bend ET 3rd bend.; wing torsion	(18) 8.64	(15) 8.65	(10) 8.39		(6) 8.06
Fuselage 3rd bend ET 3rd bend.; RCS, wing pitch	(19) 8.45	(16) 8.46	(11) 8.59		
ET bending	(20) 9.58			(11) 9.34	

[a] RCS = Reaction Control System pod.

TABLE 4. – NATURAL FREQUENCY AND MODE INDEX SUMMARY, ANTISYMMETRIC MODES

Mode	Natural frequency, Hz and (mode index)				
	Structural configuration				
	A Complete vehicle	B Orbiter with flex. attached ET & rigid. attached SRBs	C Orbiter with flex. attached ET	D Orbiter with rigid. attached ET	E Orbiter
Fuselage local nose bending; wing roll/pitch	(1) 1.00	(1) 1.08			
SRB yaw & pitch, wing roll	(2) 1.17				
Fuselage 1st bending, wing pitch			(1) 1.20	(1) 1.21	(1) 1.34
Fuselage tail bending, wing roll/pitch	(3) 1.34	(2) 1.34	(2) 1.36	(2) 1.37	(2) 1.71
ET bending, SRB yaw, wing pitch/roll	(4) 1.46				
ET bending, SRB pitch, wing pitch/roll	(5) 1.56				
Wing 1st bending, fin bending +	(6) 1.73	(3) 1.71			
Wing 1st bending, fin bending –	(7) 2.10	(4) 2.04	(3) 2.07	(3) 2.11	(3) 2.25
Fin bending, wing bending	(8) 2.29	(5) 2.31	(4) 2.37	(4) 2.39	
ET & SRB bending, wing pitch		(6) 2.50			(4) 2.53
Fin bending, wing torsion	(9) 2.53	(7) 2.55			
RCS			(5) 2.56	(5) 2.56	(5) 2.81
Fuselage, ET bending, wing pitch	(10) 2.80		(6) 2.77	(6) 2.83	
Fuselage 2nd bending, wing pitch	(11) 2.94	(8) 2.85	(7) 2.89	(7) 2.90	(6) 3.08
SRB bending, wing heave		(9) 3.19			
Fuselage 3rd bending, wing pitch, fin bending	(12) 3.44	(10) 3.67	(8) 3.92	(8) 3.98	
SRB 1st v. bending, wing heave, fin bending	(13) 3.97				
SRB 1st l. bending, wing heave, fin bending	(14) 4.07		(9) 4.39	(9) 4.49	
Wing roll, RCS pitch, wing torsion	(15) 4.33	(11) 4.36	(10) 4.52	(10) 4.92	(7) 4.35
Fuselage 3rd bending, ET 2nd bend., wing torsion	(16) 4.78	(12) 4.66			
Fuselage 4th bending, wing pitch, torsion	(17) 5.26	(13) 5.30	(11) 5.28	(11) 5.38	(8) 5.24
Fuselage 4th bending, RCS pitch	(18) 5.51				
Fuselage 5th bending, RCS pitch, wing roll	(19) 6.14	(14) 6.09	(12) 6.09	(12) 6.27	(9) 5.54

TABLE 5
GENERALIZED MASSES FOR MODES
OF THE COMPLETE VEHICLE

Mode index (a)	Generalized mass, kg (lb)			
	Symmetric		Antisymmetric	
1	33,623	(74,125)	17,815	(39,276)
2	431,670	(951,672)	60,676	(133,767)
3	173,977	(383,553)	46,235	(101,931)
4	3,873	(8,538)	395,613	(872,177)
5	8,545	(18,839)	239,945	(528,988)
6	210,721	(464,560)	4,886	(10,772)
7	17,234	(37,995)	15,132	(33,361)
8	137,304	(302,703)	1,017	(2,241)
9	8,481	(18,697)	11,107	(24,486)
10	52,404	(115,532)	8,943	(19,715)
11	3,991	(8,799)	11,848	(26,121)
12	18,213	(40,152)	13,403	(29,549)
13	14,350	(31,636)	20,904	(46,085)
14	5,001	(11,025)	56,623	(124,833)
15	27,803	(61,295)	13,142	(28,974)
16	2,749	(6,060)	8,411	(18,544)
17	14,002	(3,087)	9,921	(21,873)
18	13,112	(28,908)	18,234	(40,199)
19	1,741	(3,839)	8,038	(17,722)
20	17,527	(38,641)	6,461	(14,243)

[a]See Table 4.

TABLE 6

RATIOS OF GENERALIZED AERO FORCES OF REFERENCE MODELS

Model number (see Figure 5 and 6)	Ratio: $Q_{R,S}$ of model at flutter to that of reference model					
	$Q_{1,1}$		$Q_{1,2}$		$Q_{2,2}$	
	Real	Imag	Real	Imag	Real	Imag
	Cross section model					
1	0.992	0.990	0.980	1.026	0.941	0.999
2	1.006	1.001	1.000	.903	.972	.975
3	.995	.998	.994	1.016	.989	1.006
4	.999	.999	.998	.995	.998	.999
5	.999	.999	.998	1.006	.998	1.001
6	1.000	1.000	.999	.992	1.001	.998
7 (Reference model)	1.000	1.000	1.000	1.000	1.000	1.000
	Fuselage spanwise panel model					
8 (Reference model)	1.000	1.000	1.000	1.000	1.000	1.000
9	1.003	1.000	1.000	.998	1.001	.963

TABLE 7. – FLUTTER ANALYSIS RUN NUMBERS

Aerodynamic configuration	Run number				
	Structural configuration				
	A Complete vehicle	B Orbiter with flex. attached ET & rigid. attached SRBs	C Orbiter with flex. attached ET	D Orbiter with rigid. attached ET	E Orbiter
1. Wing alone	1A				
2. Wing & refl of fuselage	2A				
3. Wing & refl & slender body of fuselage	3A		3C		
4. Wing, fuselage & ET refl & slender body	4A	4B		4D	
5. Wing, fuselage, ET; & SRB refl only	5A				5E
6. Complete aero of orbiter, ET & SRBs	6A				6E
7. Wing aero plus refl effects of all bodies	7A				
8. Complete aero with vertical separation of SRBs halved	8A				

TABLE 8 – MAJOR MODAL CONTRIBUTIONS TO EIGENVECTORS OF PRINCIPAL FLUTTER INSTABILITIES, SYMMETRIC ANALYSES

Mode index (a)	Contribution					
	Root 7		Root 9		Root 11	
	Real	Imag	Real	Imag	Real	Imag
	RUN 1A[b]					
4	0.13	0.14	-0.27	-0.08	0.17	0.02
5	-.09	-.09	.10	.03	-.09	-.01
7	1.00	.00	–	–	–	–
9	-.03	-.02	1.00	.00	.02	–
10	–	–	–	–	1.00	–
11	-.03	-.02	.15	.01	-.82	.04
16	-.03	-.01	.10	-.01	-.28	.03
17	–	–	-.06	–	.08	-.01
	RUN 6A[b]					
4	0.12	0.21	-0.59	-0.14	0.19	–
5	-.16	-.13	.12	.06	-.14	-0.01
7	1.00	.00	.12	-.03	–	–
9	-.08	-.06	1.00	.00	-.24	-.04
10	–	–	–	–	1.00	-.00
11	-.03	-.03	.17	–	-.93	.07
16	–	–	.09	-.03	-.38	.05
17			-.10	-.01	.07	-.04

[a] See Table 4.

[b] See Table 7.

TABLE 9. – MAJOR MODAL CONTRIBUTIONS TO EIGENVECTORS OF PRINCIPAL FLUTTER INSTABILITIES, ANTISYMMETRIC ANALYSES

Mode Index (a)	Contribution									
	Root 9		Root 10		Root 11		Root 12		Root 13	
	Real	Imag	Real	Imag	Real	Imag	Real	Imag	Real	Imag
	RUN 1A[b]									
6	-0.05	-0.07	-0.17	-0.07	0.04	0.04	-0.10	-0.07	0.30	-0.02
7	-.04	-.04	-.10	-.02	–	–	-.04	-.02	.13	-.03
8	-.29	-.28	-.64	-.08	.14	.16	-.24	-.10	.62	-.18
9	1.00	.00	-.14	.00	–	–	–	–	–	–
10	.18	.14	1.00	.00	.13	0.45	-.27	-.07	.62	-.21
11	–	–	.04	.02	1.00	.00	–	–	–	–
12	–	–	.05	.01	–	–	1.00	.00	1.00	00
13	–	–	–	–	–	–	–	–	.06	-.08
15	–	–	.09	.01	-.05	-.05	.19	.03	-.58	.34
	RUN 6A[b]									
6	0.19	0.06	-0.12	-0.08	0.07	-0.01	–	-0.20	–	-0.11
7	.16	.00	-.12	.00	–	–	–	–	–	–
8	1.00	.00	-.66	-.05	.21	-.03	-0.19	-.36	-0.06	-.20
9	-.43	.80	-.86	-.06	–	–	–	–	–	–
10	-.82	.27	1.00	.00	-.29	-.04	-.28	-.33	-.15	-.16
11	-.13	.00	.19	.02	1.00	.00	–	–	–	–
12	–	–	–	–	–	–	1.00	.00	1.00	0.00
13	–	–	–	–	–	–	–	–	–	–
15	–	–	–	–	–	–	–	.22	.06	.13

[a] See Table 4.

[b] See Table 7.

TABLE 10.– RATIOS OF FLUTTER SPEED TO FLUTTER SPEED OF WING ALONE

Run no. (a)	Ratio: Flutter speed/reference flutter speed[b]					
	Root 7	Root 9[c]	Root 10	Root 11	Root 12	Root 13
1A	[–]	1.00 [1.00]	1.00	1.00 [1.00]	1.00	1.00
2A	[–]	.92 [.985]	.96	.95 [1.01]	.99	1.00
3A	[1.00]	– [.97]	.94	.72 [1.00]	.98	.97
4A	[1.07]	– [.95]	.93	.72 [1.00]	.98	.97
5A	[–]	– [.91]	.90	.70 [.98]	.94	.94
6A	[–]	– [.91]	.89	.70 [.98]	.94	.94
7A	[1.07]	.87 [.94]	.92	.92 [.98]	.97	.97
8A	[–]	– [.91]	.89	.70 [.98]	.94	.94

[a] See Table 7.

[b] Use flutter speed of run no. 3A for root 7 and flutter speed of run no. 1A for roots 9, 10, 11, 12 & 13.

[c] Root 9 is stable for run no.'s 3A, 4A, 5A, 6A, and 8A – antisymmetric.

Note: Numbers in brackets refer to symmetric configurations. Numbers without brackets refer to antisymmetric configurations.

TABLE 11. – NONDIMENSIONAL GENERALIZED AERO FORCES NEAR FLUTTER, ANTISYMMETRIC ANALYSES

Run no. (a)	Roots	Generalized aero forces, nondimensional											
		Wing panels alone[b]				Wing & interf panels[b]				All elements[b]			
	$Q_{R,S}$ → / ↓	8	9	10	11	8	9	10	11	8	9	10	11
6A	8	0.008 (.008)	-0.013 (-.002	-0.055 (.011)	-0.007 (.003)	0.009 (.008)	-0.011 (-.001)	-0.045 (.012)	-0.014 (-.008)	0.009 (.009)	-0.010 (-.001)	-0.041 (.011)	0.004 (-.009)
	9	.009 (.004)	-.014 (.003)	-.072 (.014)		.007 (.004)	-.016 (.005)	-.058 (.014)		.005 (.003)	-.030 (.008)	-.066 (.019)	
	10	.057 (.040)	-.088 (-.001)	-.440 (.094)	-.101 (.013)	.061 (.042)	-.071 (.005)	-.349 (.102)	-.193 (-.024)	.068 (.043)	-.088 (.066)	-.768 (.106)	-.515 (-.022)
	11	-.001 (-.004)		-.080 (-.016)	-.051 (.011)	.005 (-.001)		-.053 (-.001)	-.105 (-.002)	.017 (.001)		-.370 (-.021)	-.422 (.023)
7A	8	0.009 (.008)	-0.013 (-.002)	-0.056 (.013)	-0.006 (-.002)								
	9	.007 (.003)	-.013 (.002)	-.065 (.015)									
	10	.056 (.039	-.090 (.001)	-.459 (.109)	-.113 (.020)								
	11	-.001 (-.003)		-.123 (-.026)	-.070 (.008)								
1A	8	0.008 (.008)	-0.011 (-.002)	-0.045 (.012)									
	9	.006 (.003)	-.008 (.001)	-.039 (.012)	-.007 (.005)								
	10	.050 (.038)	-.070 (-.002)	-.328 (.093)	-.071 (.006)								
	11	-.002 (-.003)		-.067 (-.020)	-.046 (.007)								

[a] See table 7.

[b] See figure 4.

Note: Numbers in ( ) are imaginary components of the generalized forces.

TABLE 12. – NONDIMENSIONAL GENERALIZED AERO FORCES NEAR FLUTTER, SYMMETRIC ANALYSES

Run no. (a)	$Q_{R,S}$	Generalized aero forces, nondimensional											
		Wing panels alone[b]				Wing & interf panels[b]				All elements[b]			
	→	4	5	9	11	4	5	9	11	4	5	9	11
6A	4	0.399 (.244)		-0.309 (.014)		0.373 (.244)		-0.405 (.029)		0.366 (.246)		-0.439 (.019)	
	5		0.159 (.138)	.058 (-.006)			0.137 (.136)	.032 (-.011)			0.119 (.148)	-.002 (-.015)	
	9	.317 (.136)	-.196 (-.123)	-.477 (.101)	-0.231 (.001)	.249 (.139)	-.277 (-.222)	-.701 (.137)	-0.247 (-.004)	.219 (-.164)	-.286 (.004)	-1.198 (.137)	-0.257 (-.016)
	11			-.111 (.081)	-.371 (.061)			-.126 (.110)	-.379 (.060)			-.127 (.112)	-.383 (.062)
7A	4	0.391 (.239)		0.285 (.010)									
	5		0.165 (.136)	.089 (-.016)									
	9	.294 (.124)	-.177 (-.017)	-.395 (.082)	-0.204 (.002)								
	11			-.112 (.082)	-.375 (.061)								
1A	4	0.315 (0.218)		-0.183 (.000)									
	5		-0.157 (.137)	.080 (-.002)									
	9	.201 (-.100)	-.140 (-.029)	-.217 (.045)	-.127 (-.002)								
	11			-.089 (.046)	-.339 (.047)								

[a] See table 7.

[b] See figure 4.

Note: Numbers in ( ) are imaginary components of the generalized forces.

TABLE 13. – FLUTTER SPEEDS FOR CONFIGURATION AND STRUCTURAL VARIATIONS

Aerodynamic configuration		Flutter speed, m/sec (kt)				
		Structural configuration				
		A Complete vehicle	B Orbiter with flex. attached ET & rigid. attached SRB	C Orbiter with flex. attached ET	D Orbiter with rigid. attached ET	E Orbiter
3. Wing & reflection & slender body of fuselage	Anti-Sym	273 (530)				273 (530)
	Sym	354 (690)				338 (655)
4. Wing & fuselage & ET reflection & slender body	Anti-Sym	270 (525)		250 (485)	237 (460)	
	Sym	346 (675)		338 (655)	309 (600)	
5. Wing; fuselage & ET reflection & slender body; SRB reflection	Anti-Sym	261 (510)	268 (515)			
	Sym	332 (645)	340 (660)			
6. Complete aero of orbiter, ET & SRBs.	Anti-Sym	258 (505)	268 (515)			
	Sym	332 (645)	340 (660)			

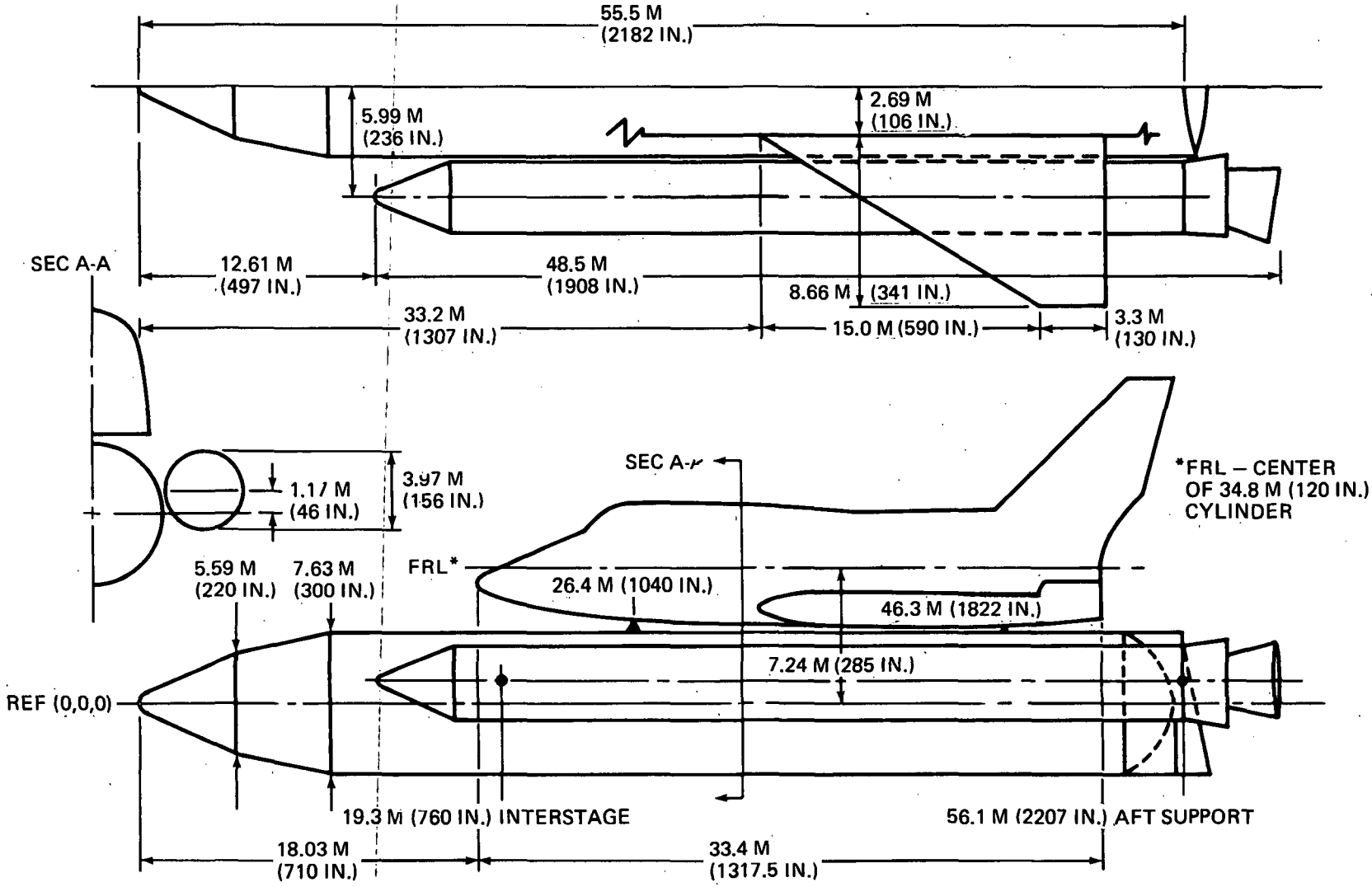

Fig. 1 Space Shuttle Geometry for G-III Design

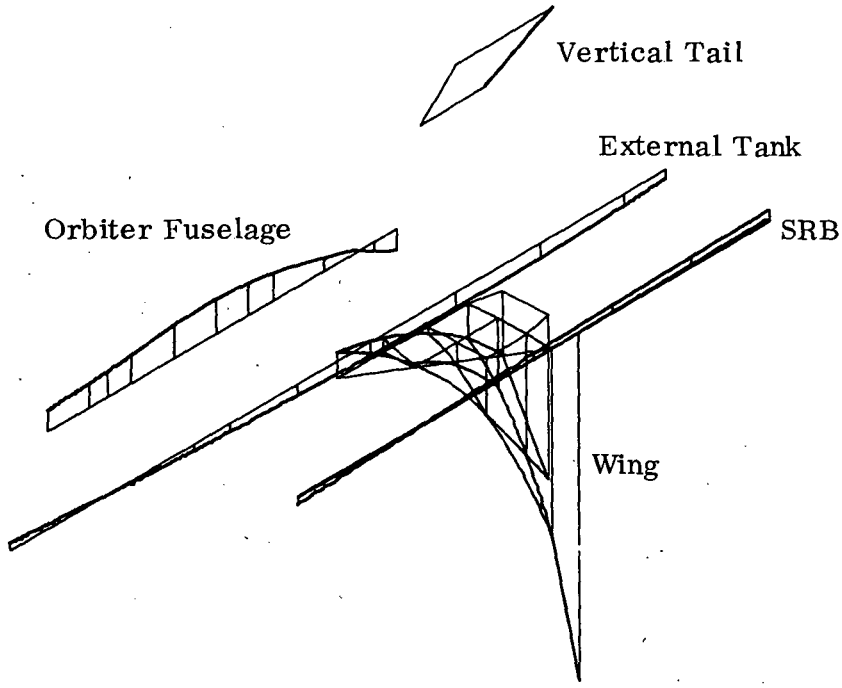

Symmetric Mode 4 (2.02 Hz)

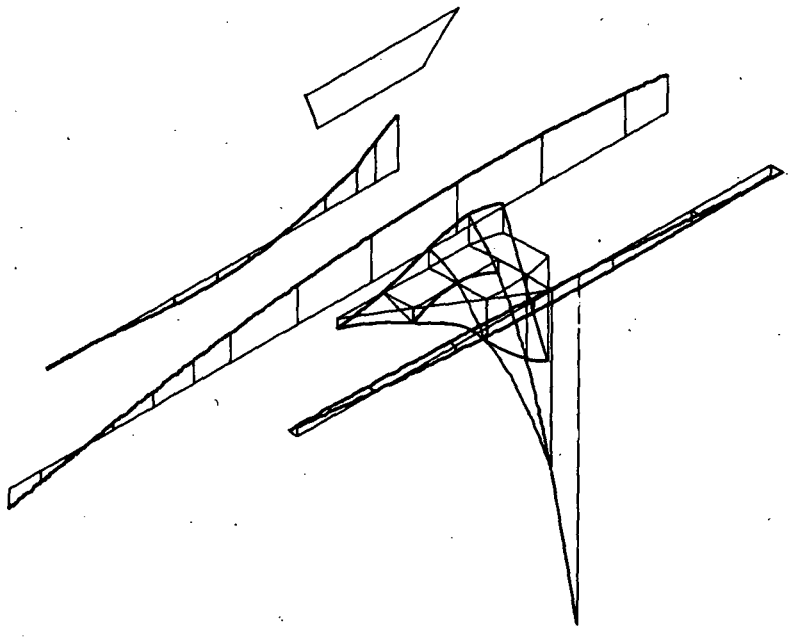

Symmetric Mode 5 (2.36 Hz)

Fig. 2 Mode Shapes of Orbiter Flexibly Attached to ET and SRB (Sheet 1 of 9)

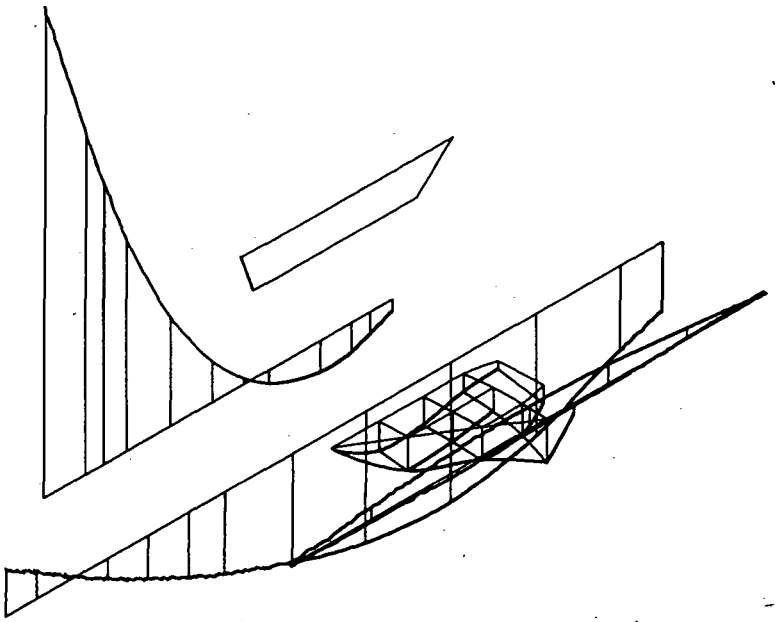

Symmetric Mode 7 (2.64 Hz)

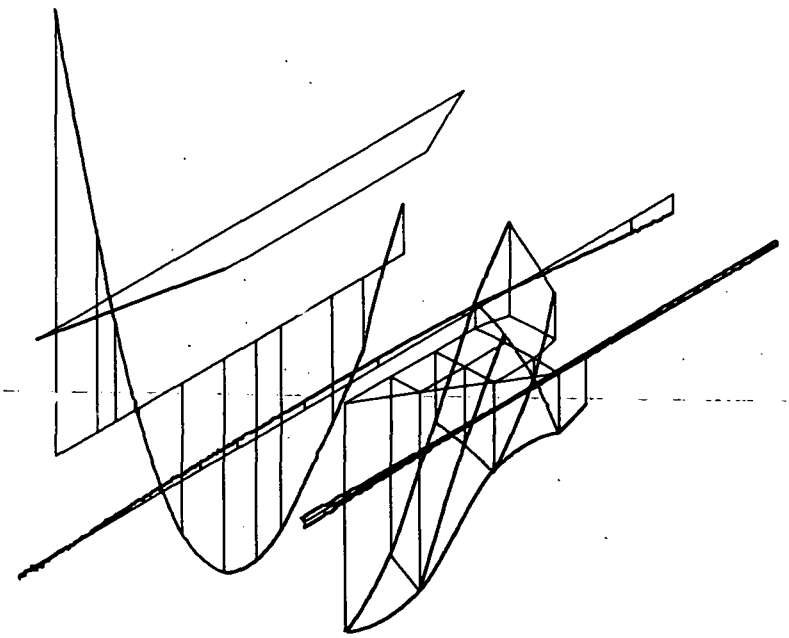

Symmetric Mode 9 (3.40 Hz)

Fig. 2 Mode Shapes of Orbiter Flexibly Attached to ET and SRB (Sheet 2 of 9)

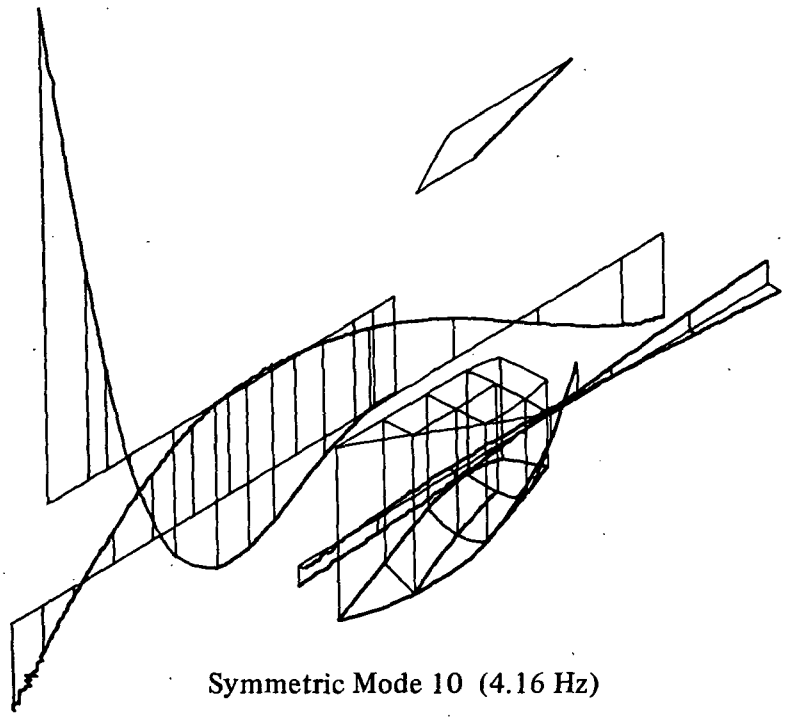

Symmetric Mode 10 (4.16 Hz)

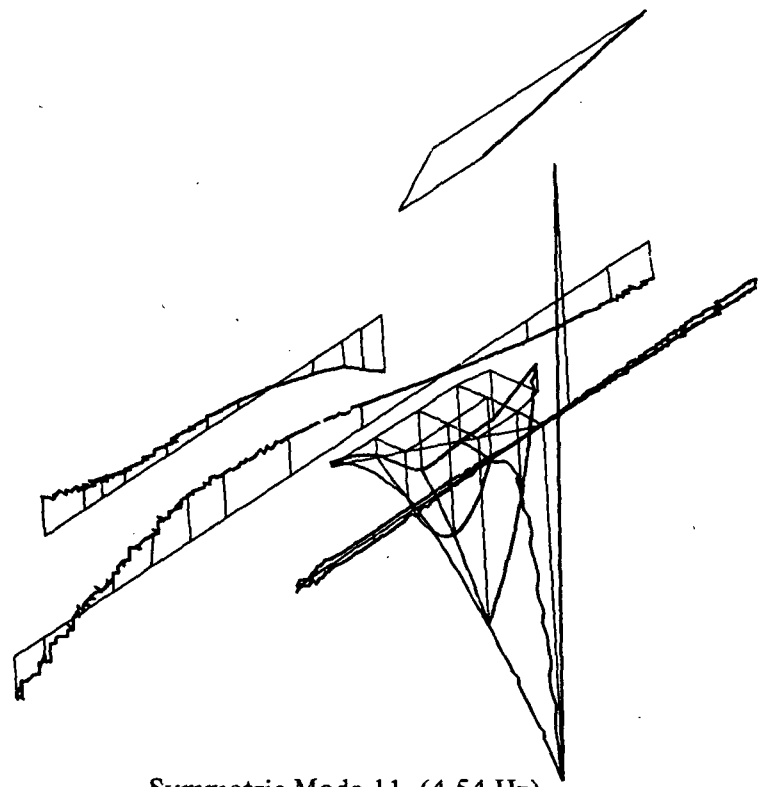

Symmetric Mode 11 (4.54 Hz)

Fig. 2 Mode Shapes of Orbiter Flexibly Attached to ET and SRB (Sheet 3 of 9)

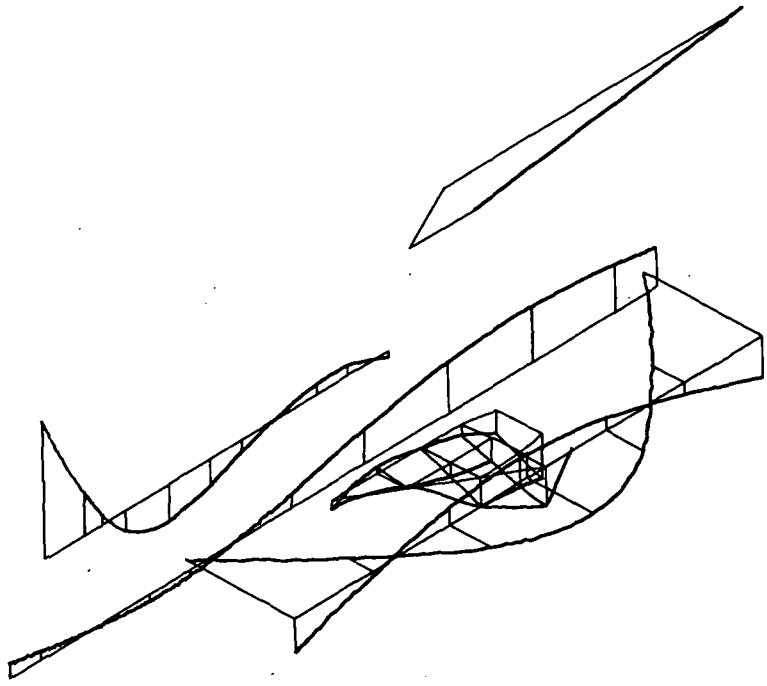

Symmetric Mode 15 (5.98 Hz)

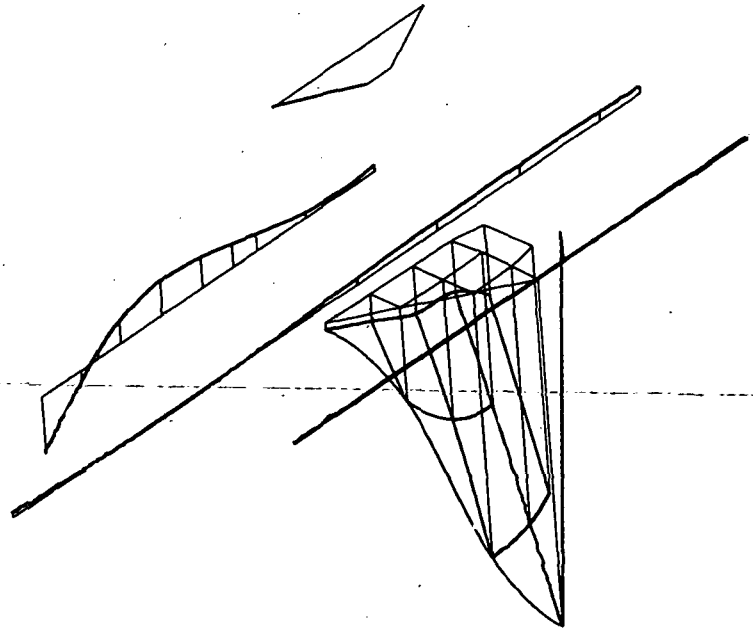

Symmetric Mode 16 (6.26 Hz)

Fig. 2 Mode Shapes of Orbiter Flexibly Attached to ET and SRB (Sheet 4 of 9)

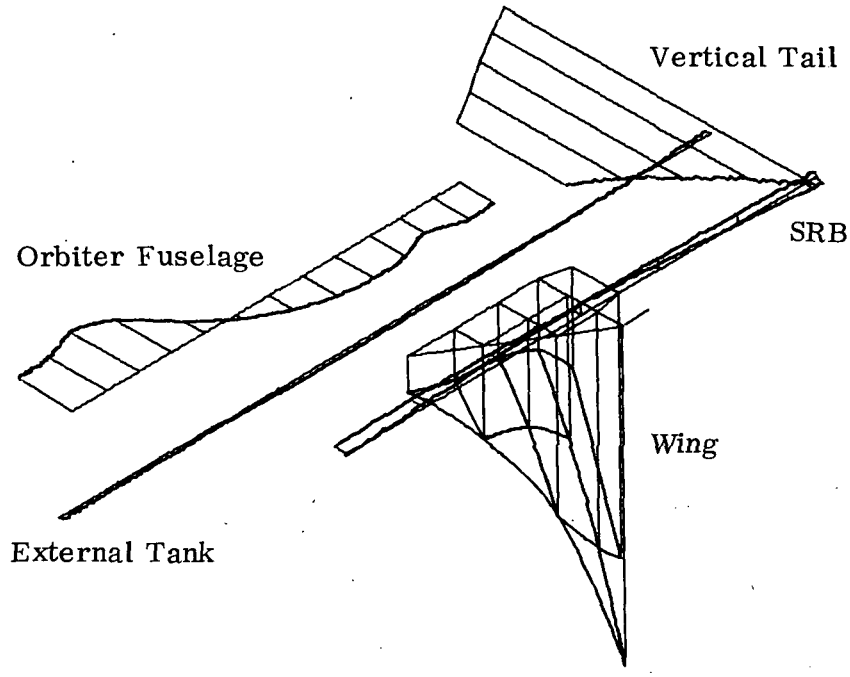

Antisymmetric Mode 6 (1.73 Hz)

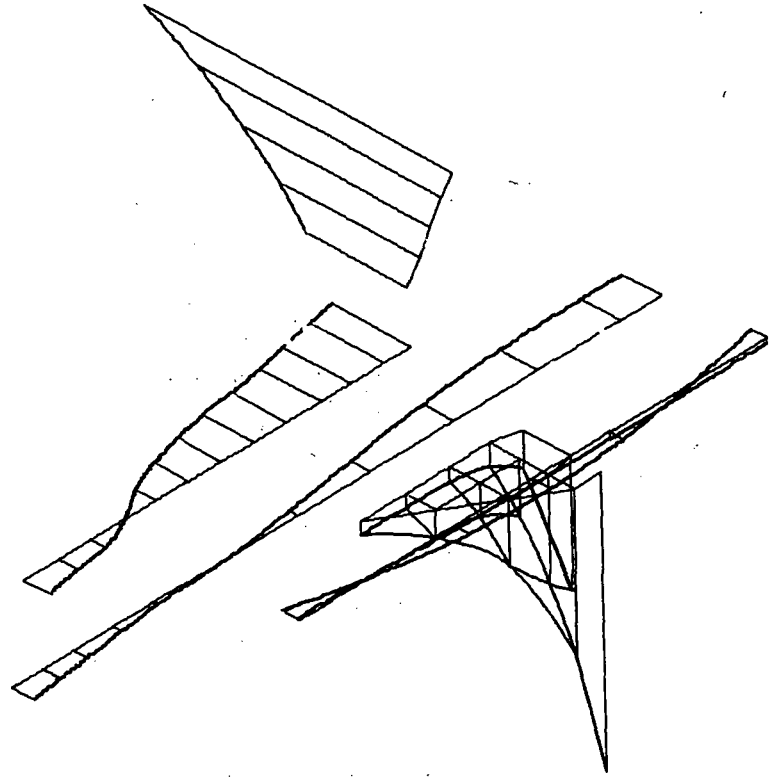

Antisymmetric Mode 7 (2.10 Hz)

Fig. 2 Mode Shapes of Orbiter Flexibly Attached to ET and SRB (Sheet 5 of 9)

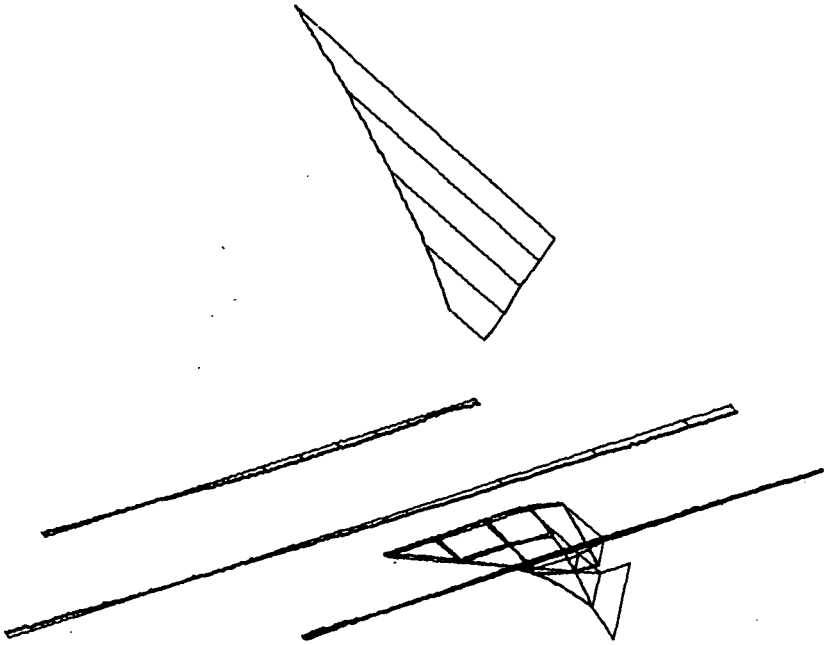

Antisymmetric Mode 8 (2.29 Hz)

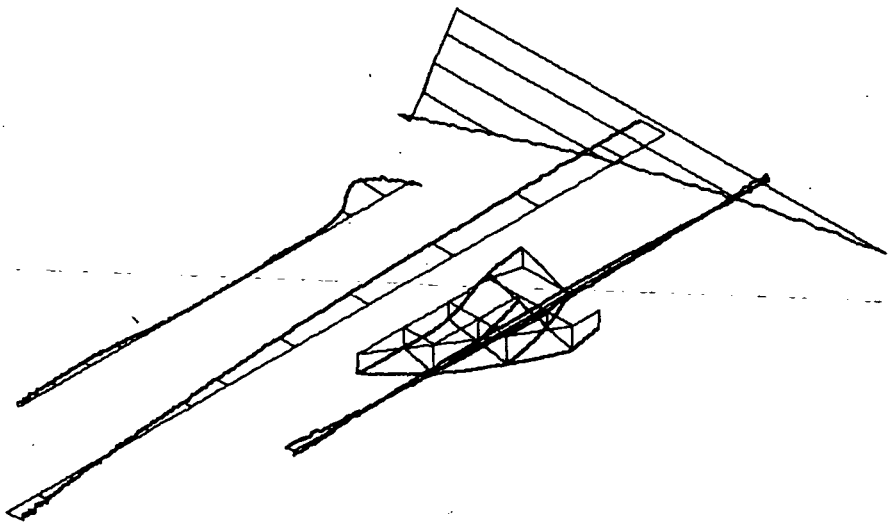

Antisymmetric Mode 9 (2.53 Hz)

Fig. 2 Mode Shapes of Orbiter Flexibly Attached to ET and SRB (Sheet 6 of 9)

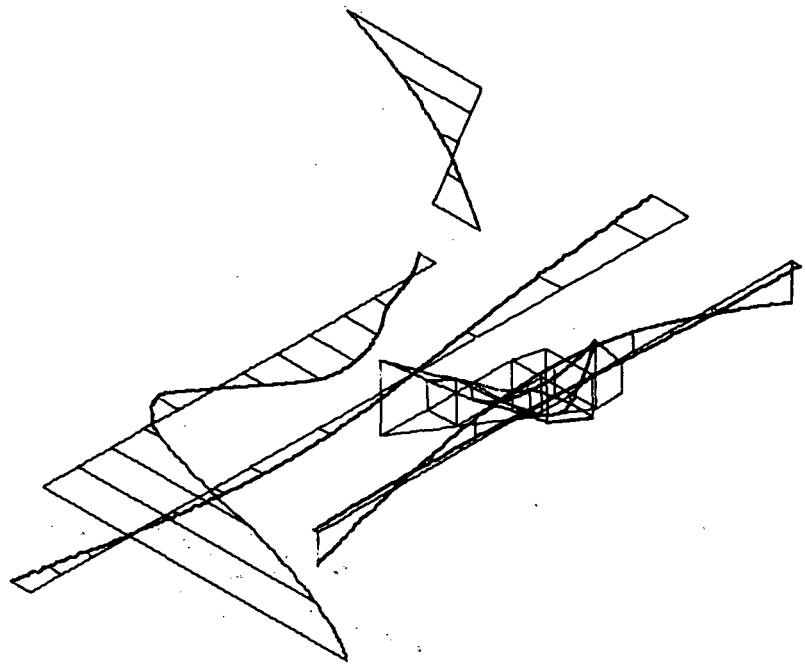

Antisymmetric Mode 10 (2.80 Hz)

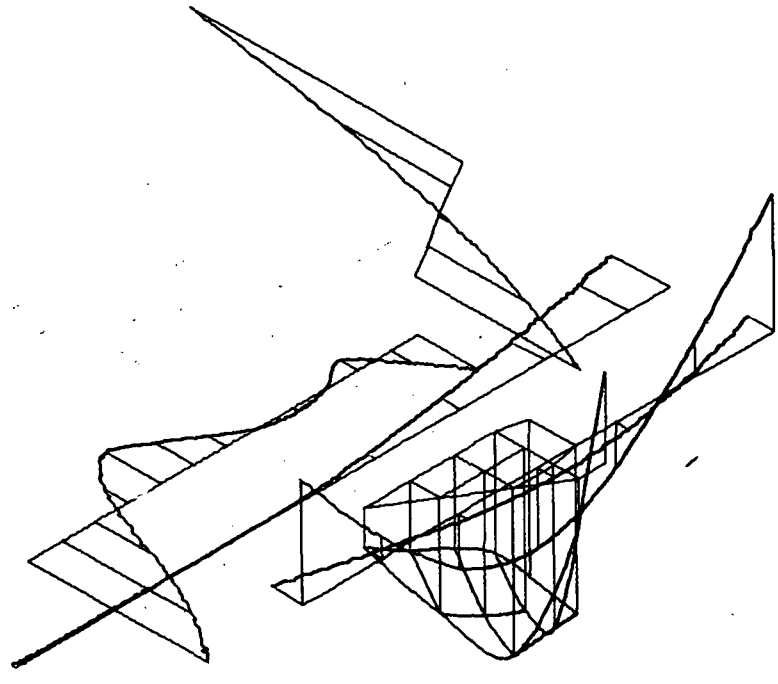

Antisymmetric Mode 11 (2.94 Hz)

Fig. 2 Mode Shapes of Orbiter Flexibly Attached to ET and SRB (Sheet 7 of 9)

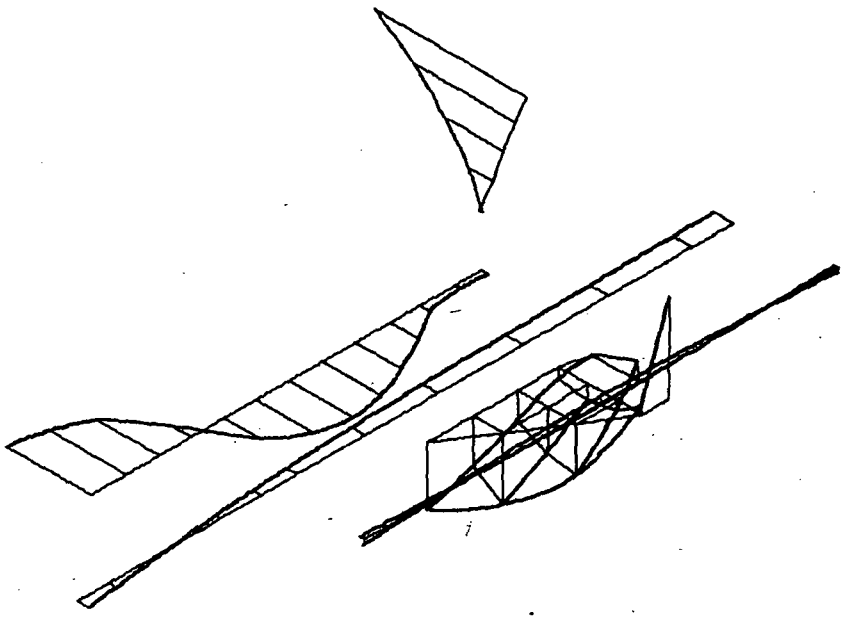

Antisymmetric Mode 12 (3.44 Hz)

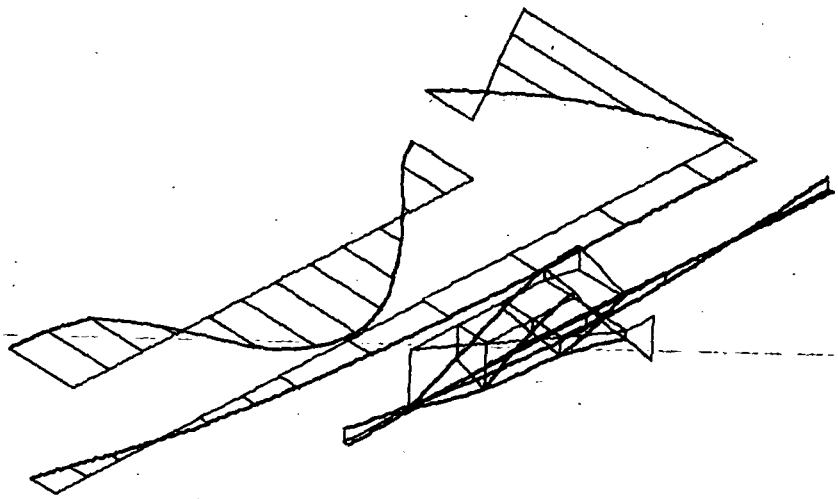

Antisymmetric Mode 13 (3.97 Hz)

Fig. 2 Mode Shapes of Orbiter Flexibly Attached to ET and SRB (Sheet 8 of 9)

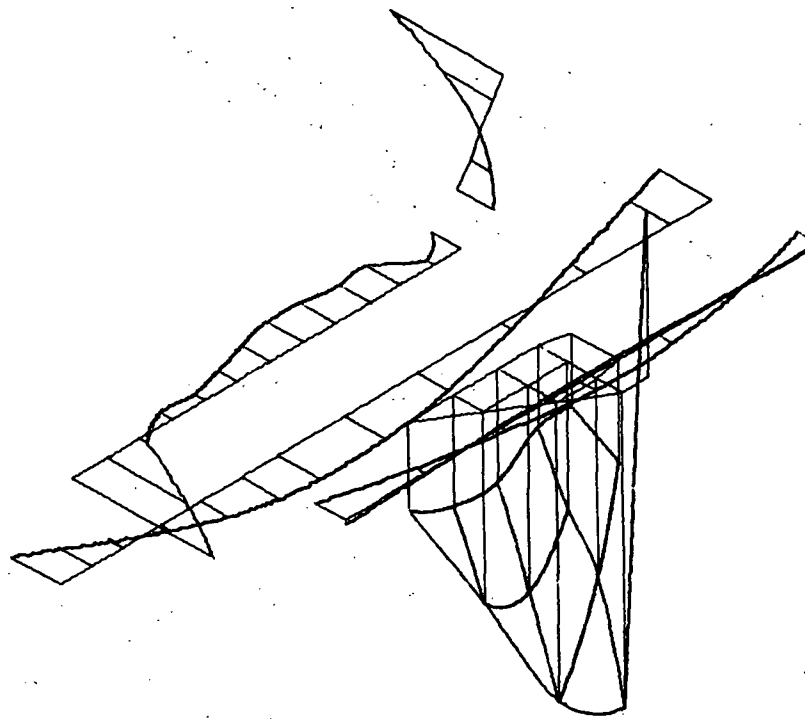

Antisymmetric Mode 15 (4.33 Hz)

Fig. 2 Mode Shapes of Orbiter Flexibly Attached to ET and SRB (Sheet 9 of 9)

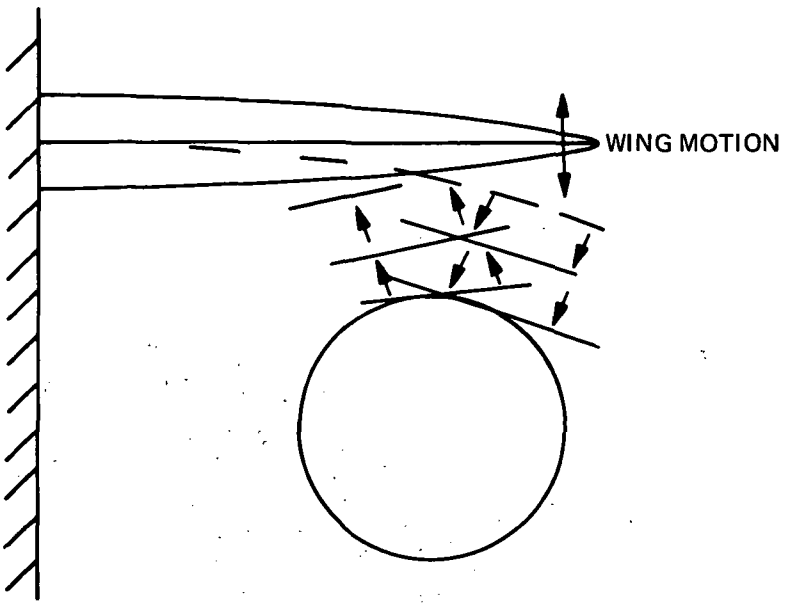

1. WING INDUCES PRESSURE ON WING
2. WING INDUCES PRESSURE ON BODY
3. PRESSURE IS REFLECTED BACK ON WING

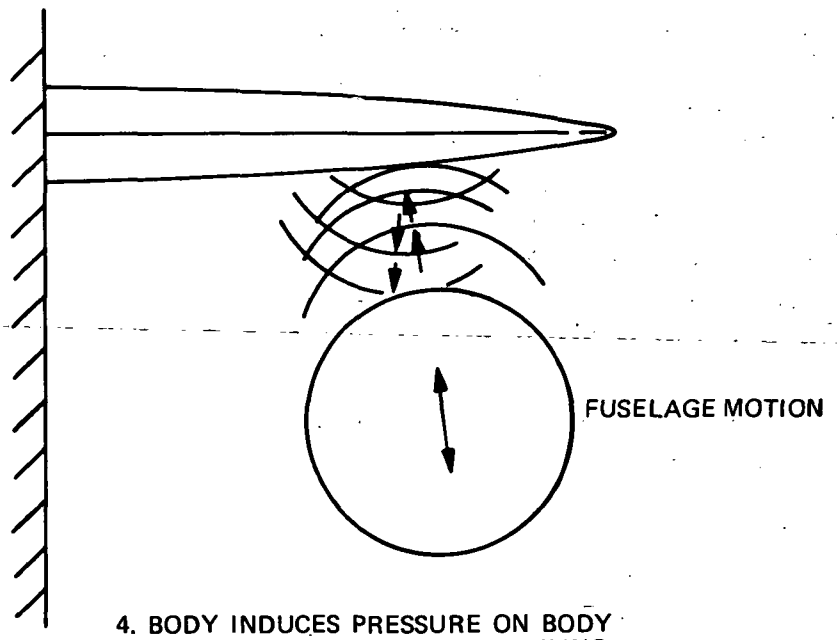

4. BODY INDUCES PRESSURE ON BODY
5. BODY INDUCES PRESSURE ON WING
6. PRESSURE IS REFLECTED BACK ON BODY

Fig. 3 Wing-Body Interaction Effects

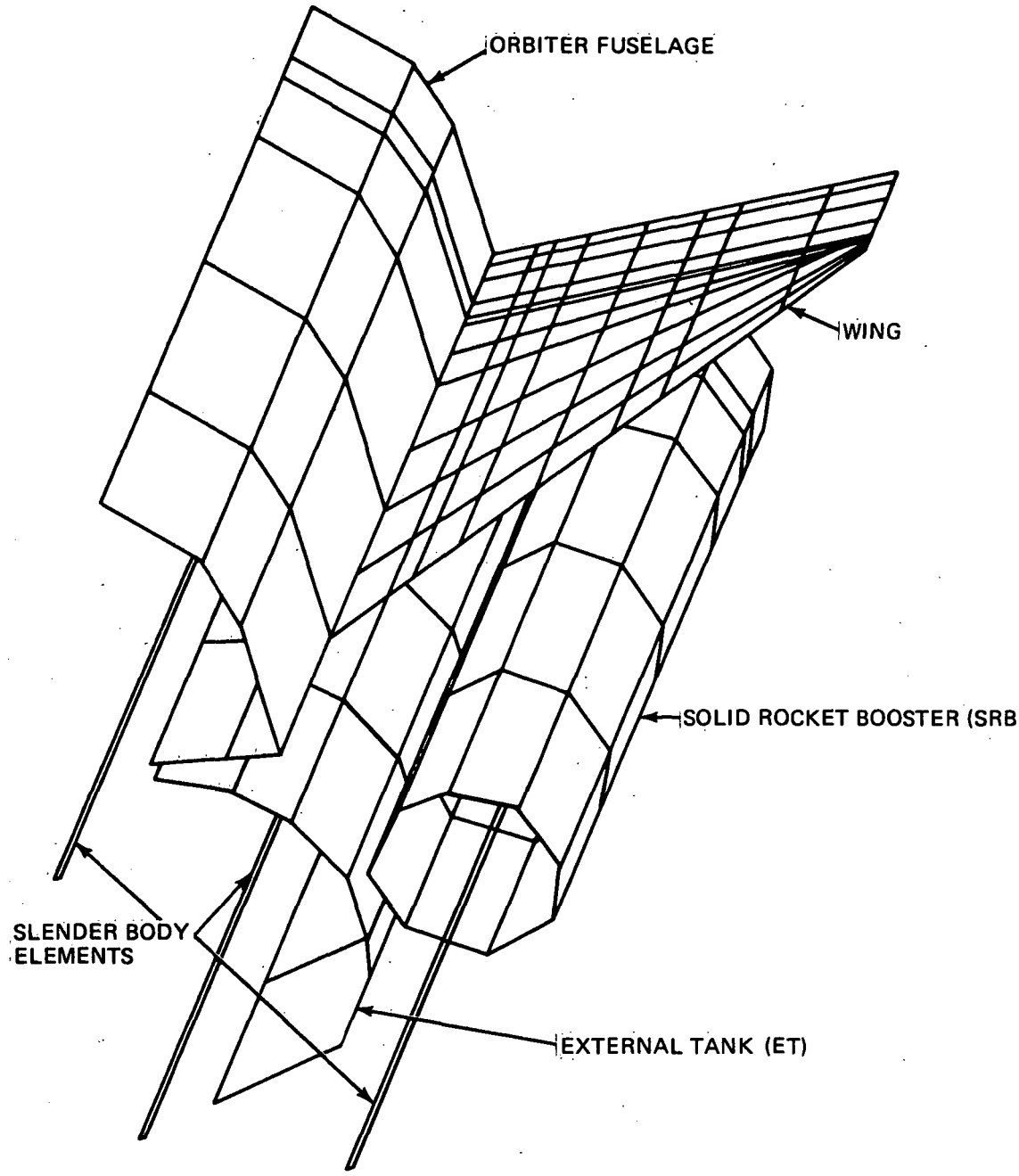

Fig. 4A Aerodynamic Model of Space Shuttle, Overall View

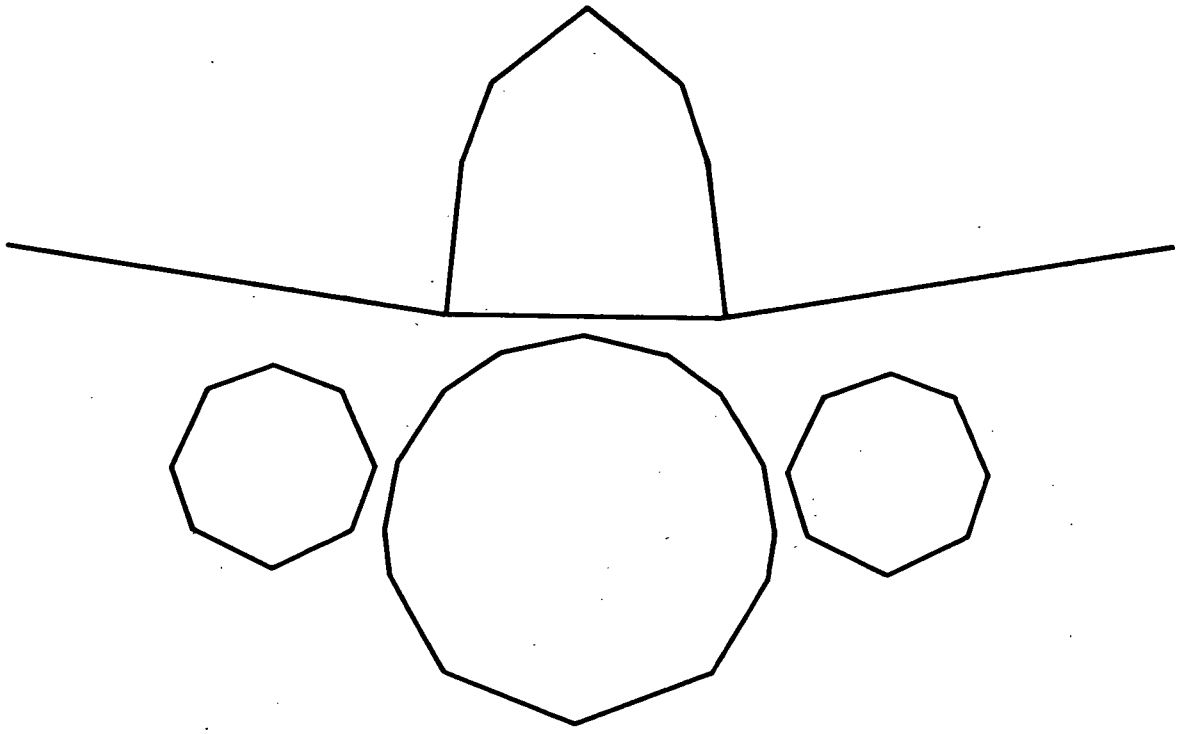

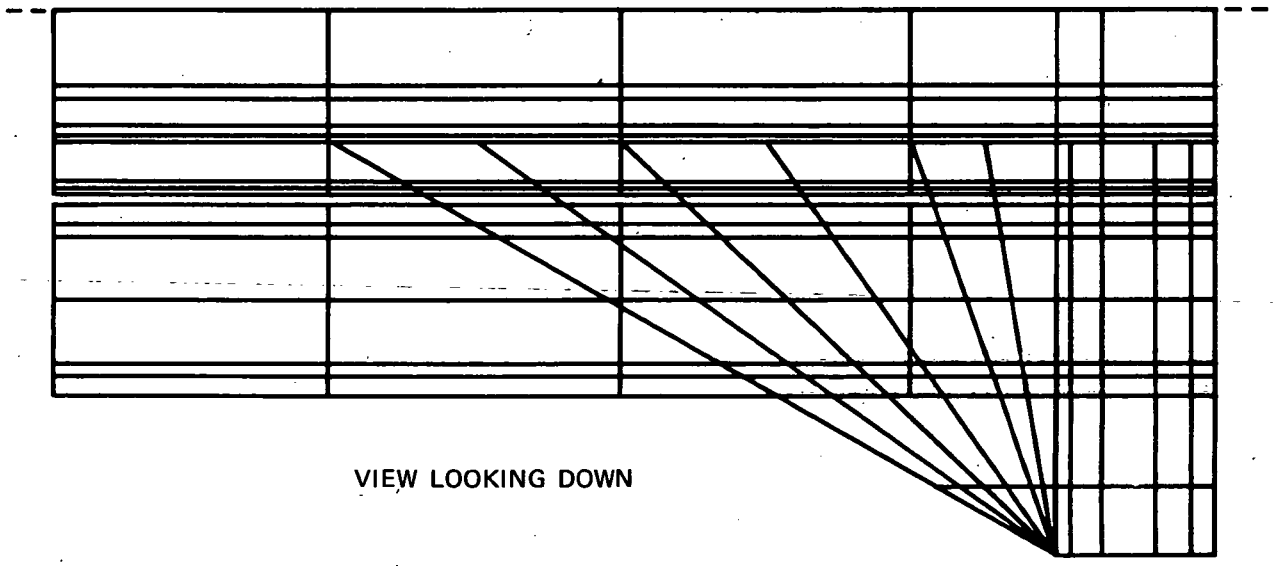

Fig. 4B Aerodynamic Model of Space Shuttle, Views Looking Aft and Down

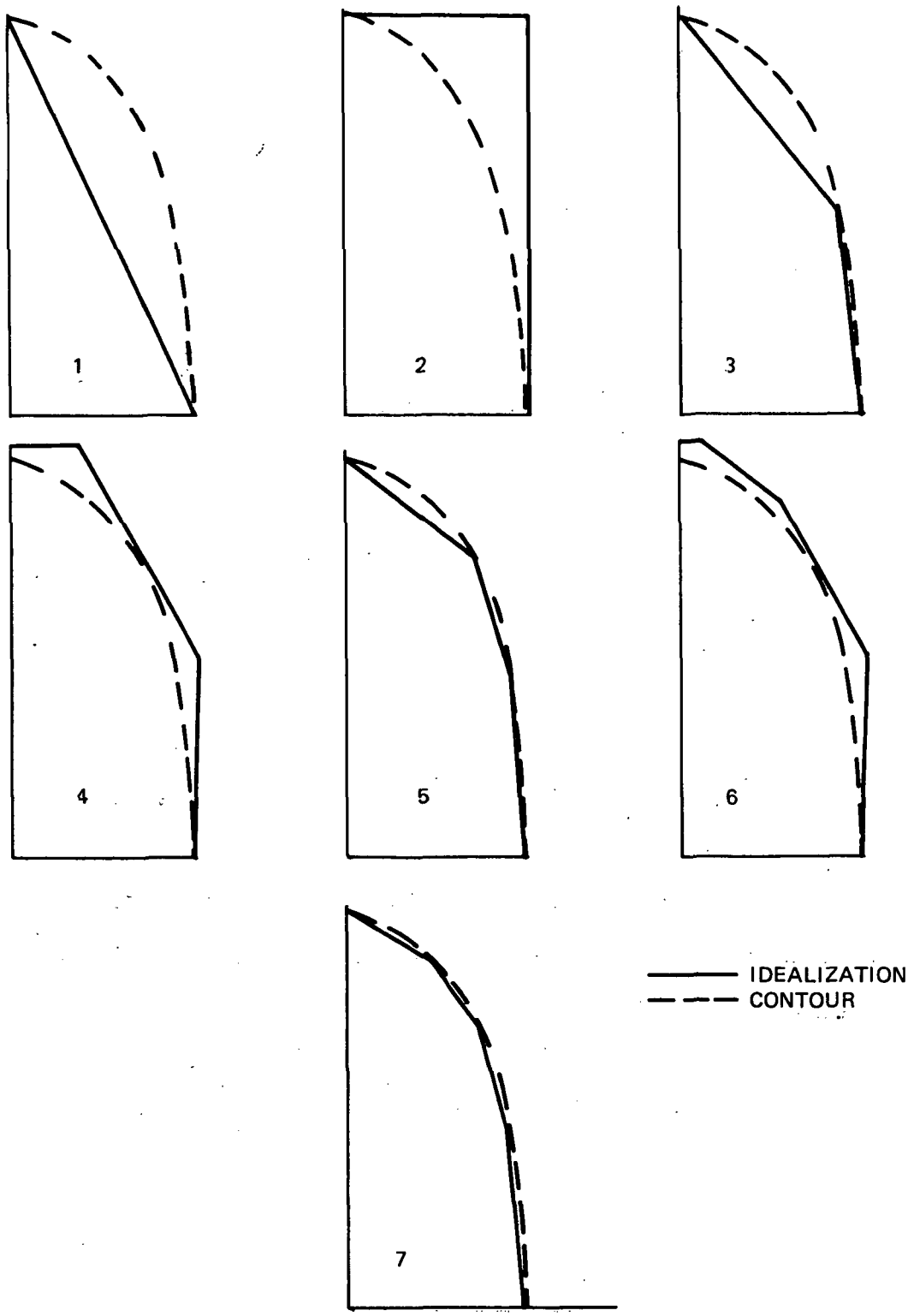

Fig. 5 Cross Section Models of Orbiter Fuselage

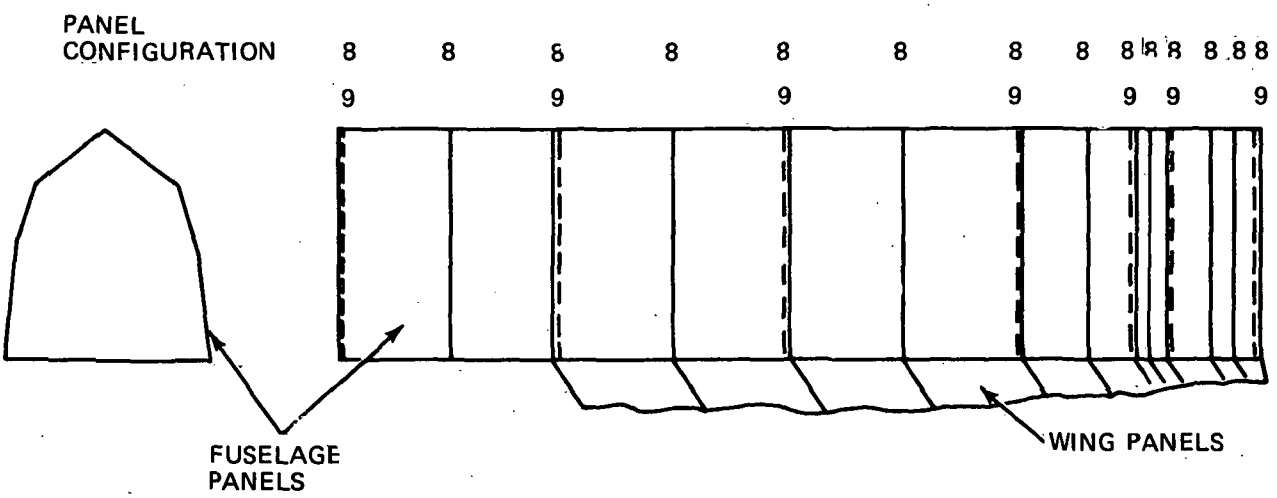

Fig. 6 Axial Panel Locations for Orbiter Fuselage

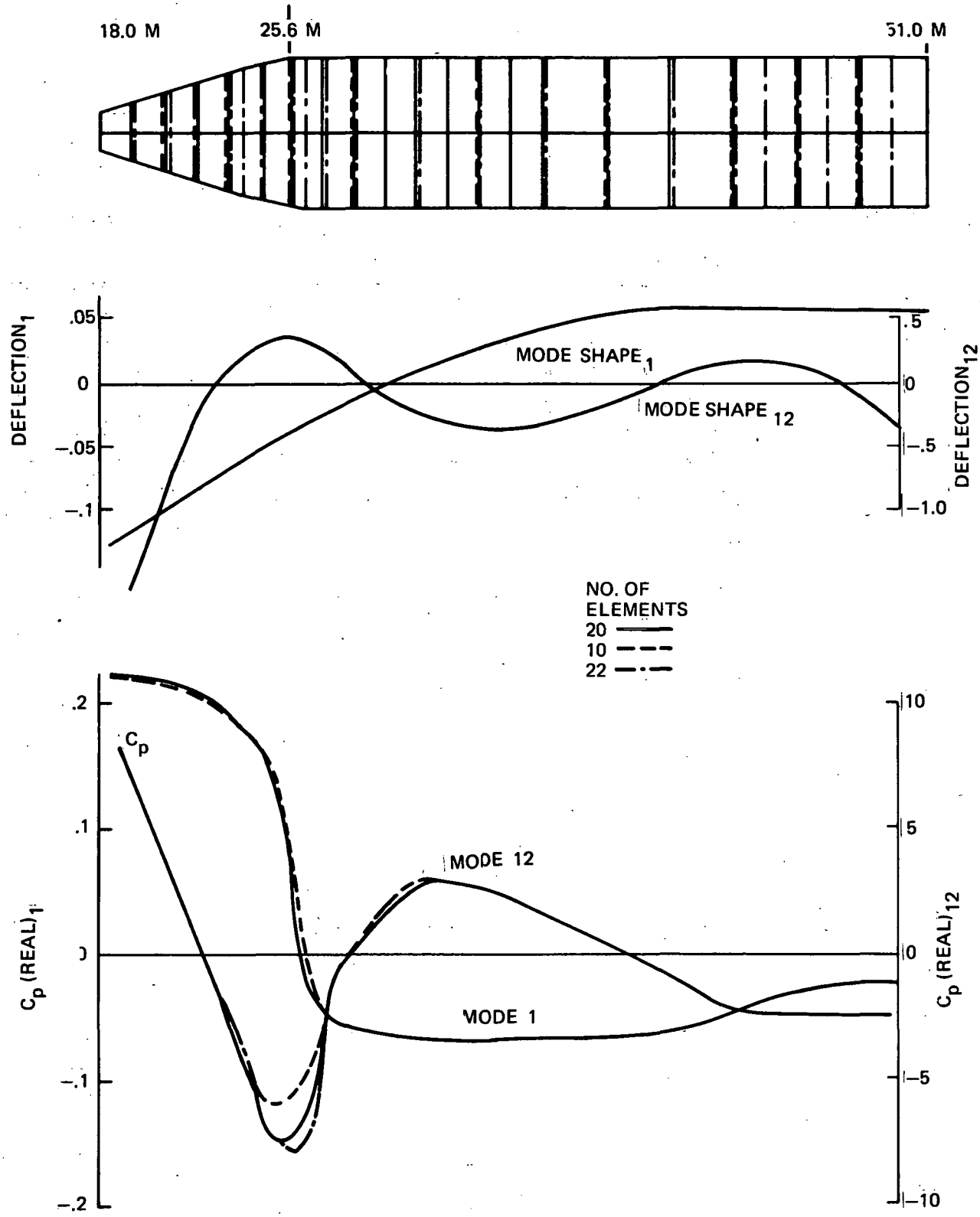

Fig. 7 Slender Body Modeling Study

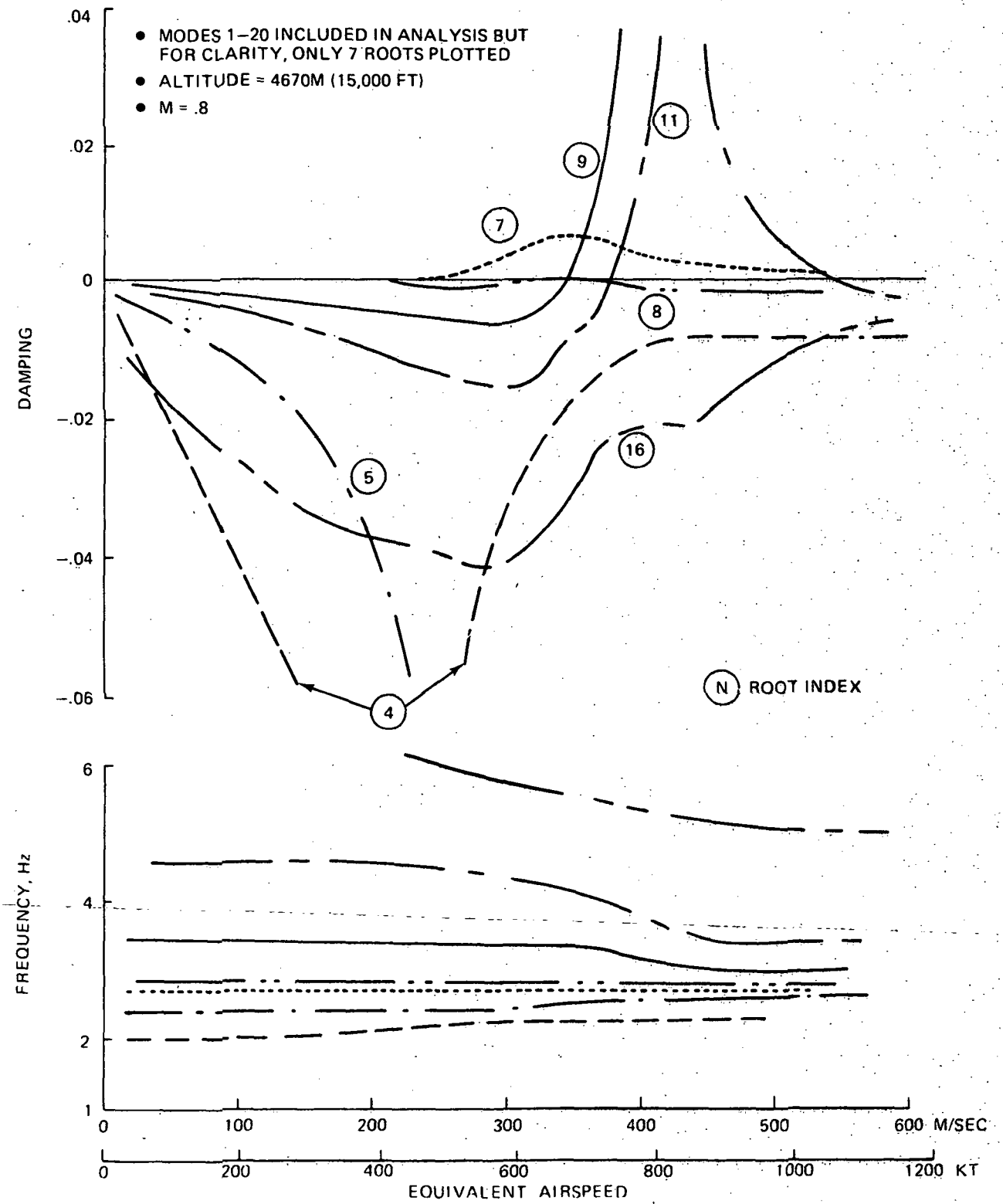

Fig. 8 V-g-f Plot for Symmetric Run 1A:
Wing Aerodynamics with Complete Vehicle Modes

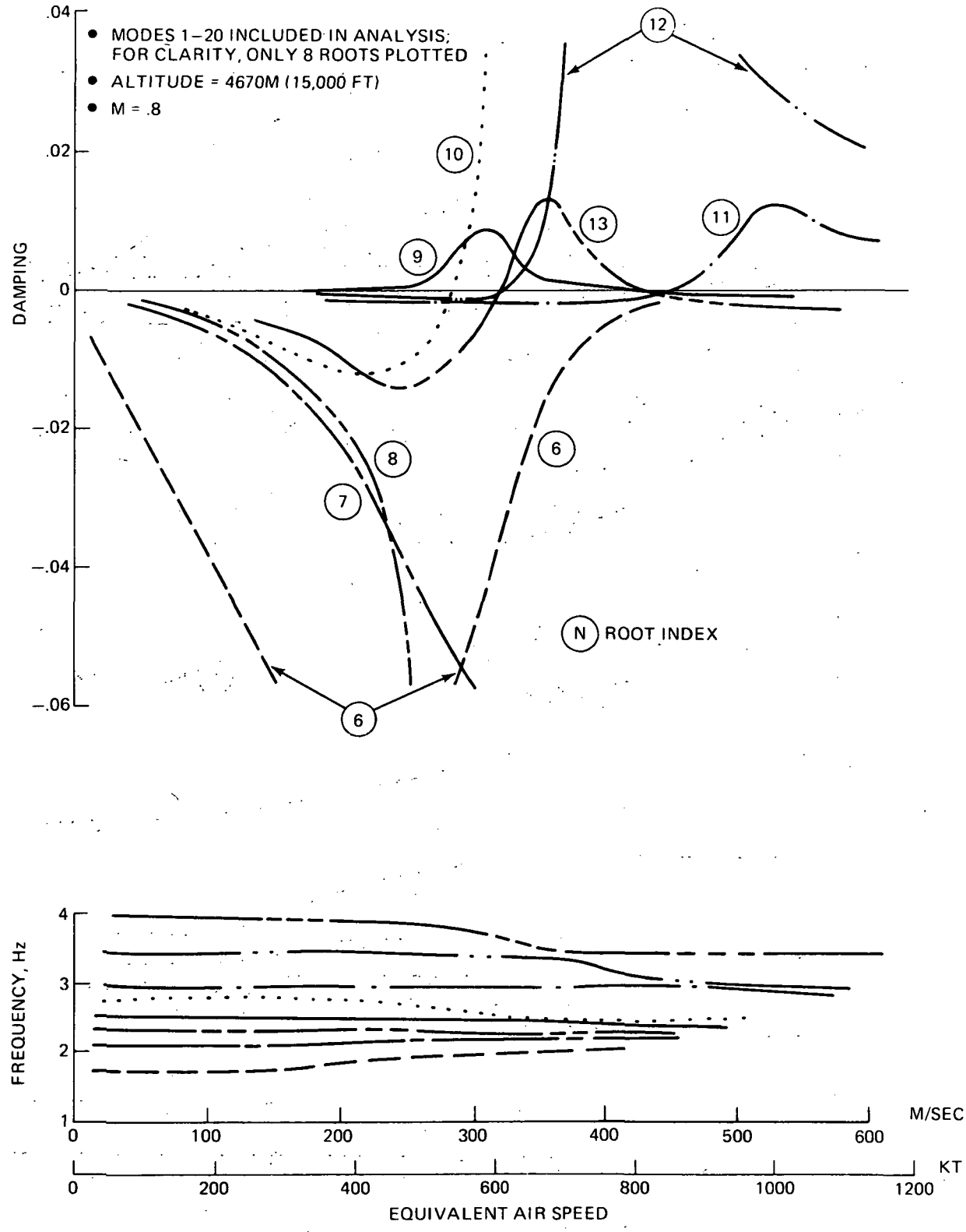

Fig. 9 V-g-f Plot for Antisymmetric Run 1A:
Wing Aerodynamics with Complete Vehicle Modes

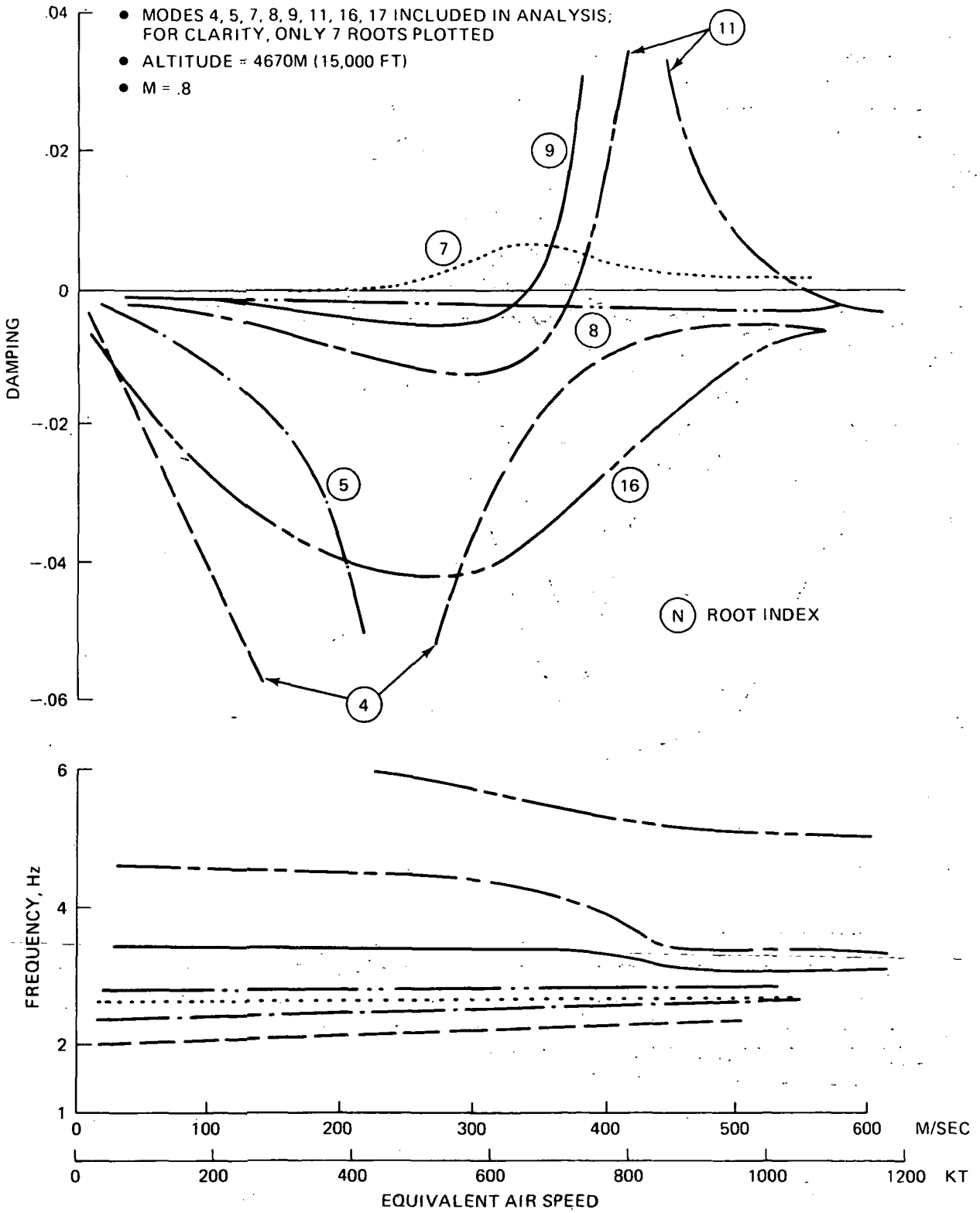

Fig. 10 V-g-f Plot for Symmetric Run 1A:
Wing Aerodynamics with Selected Complete Vehicle Modes

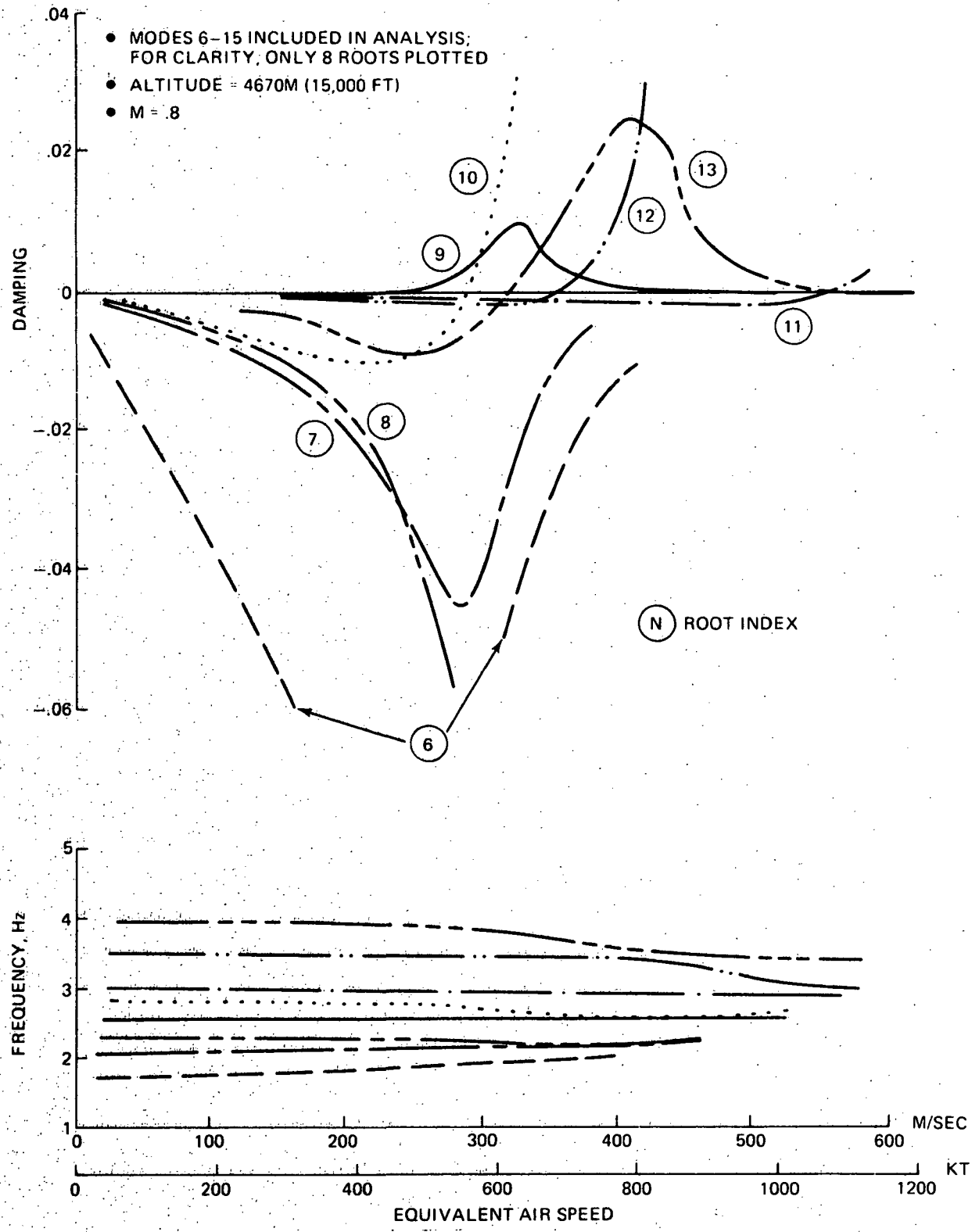

Fig. 11 V-g-f Plot for Antisymmetric Run 1A:
Wing Aerodynamics with Selected Complete Vehicle Modes

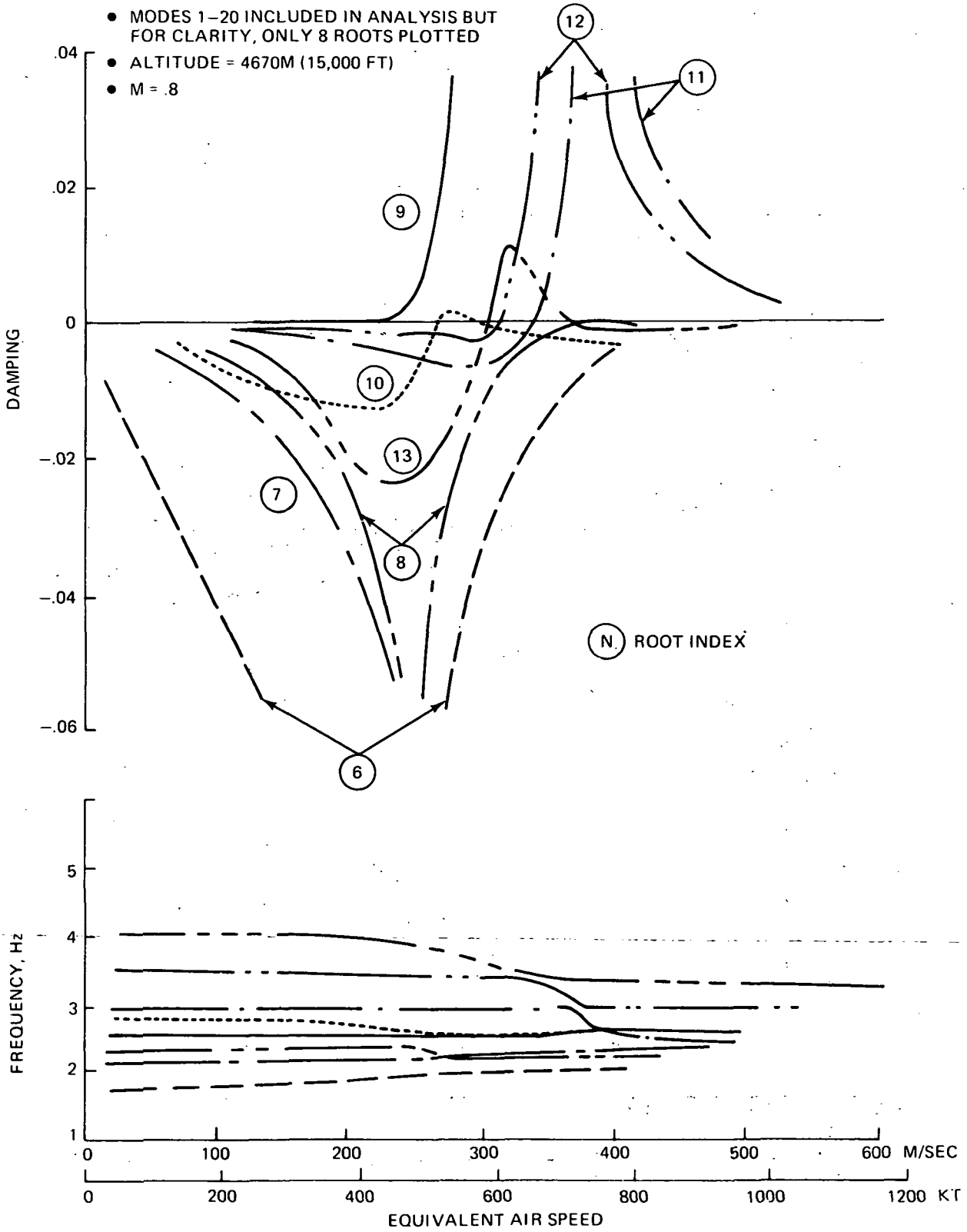

Fig. 12 V-g-f Plot for Antisymmetric Run 6A: Aerodynamics and Modes of the Complete Vehicle

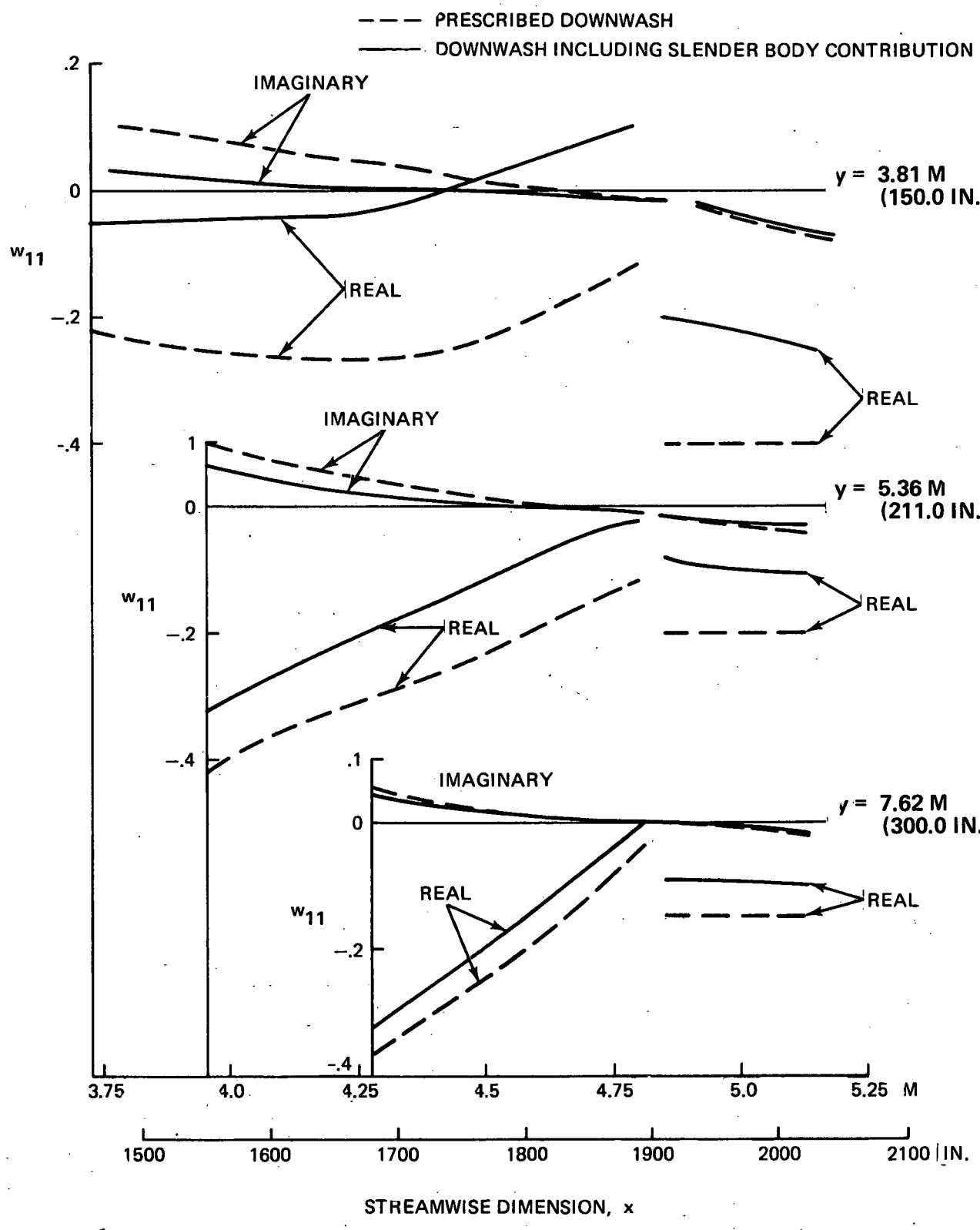

Fig. 13 Slender Body Effect on Wing Downwash

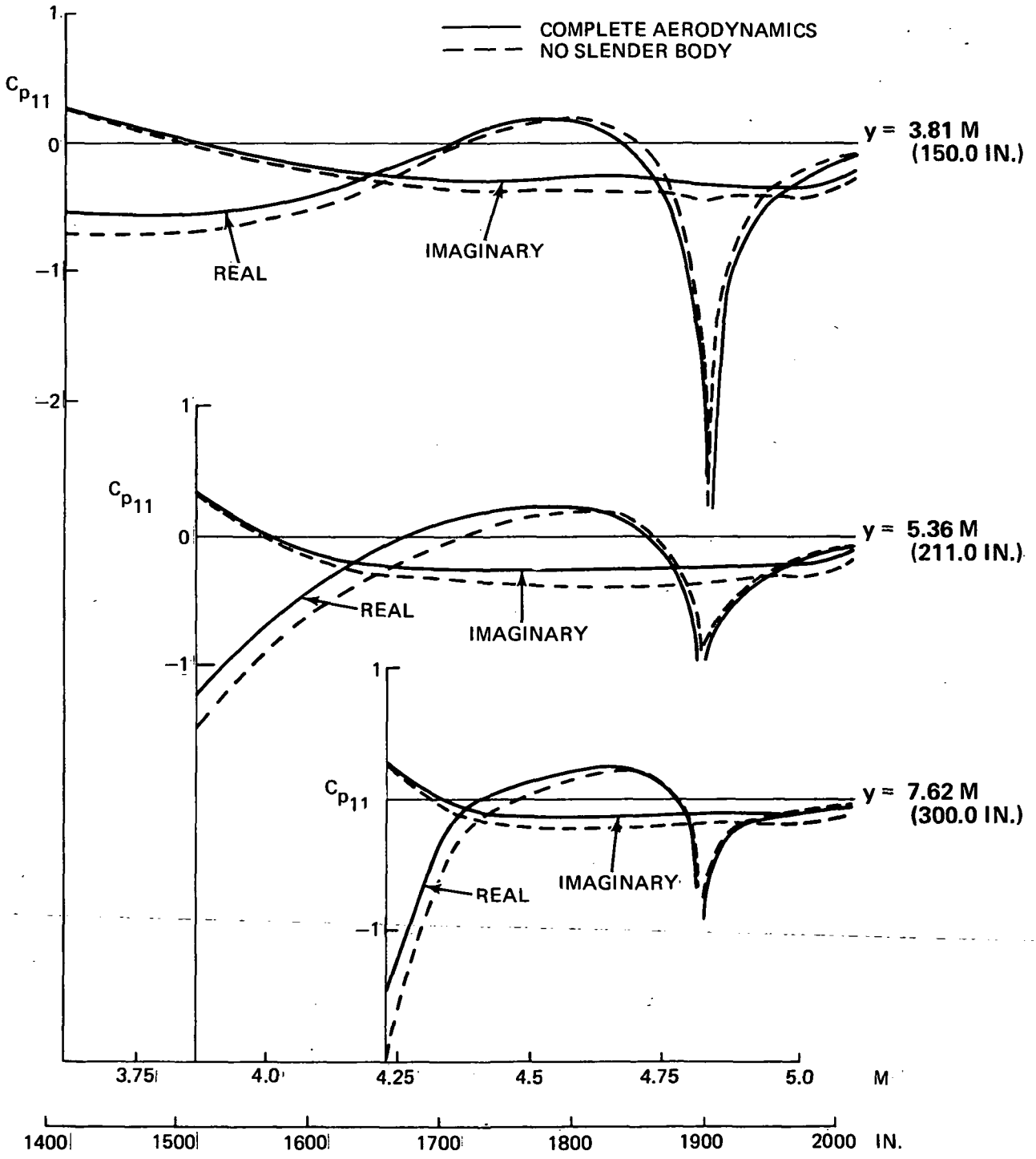

Fig. 14 Slender Body Effect on Wing Pressures

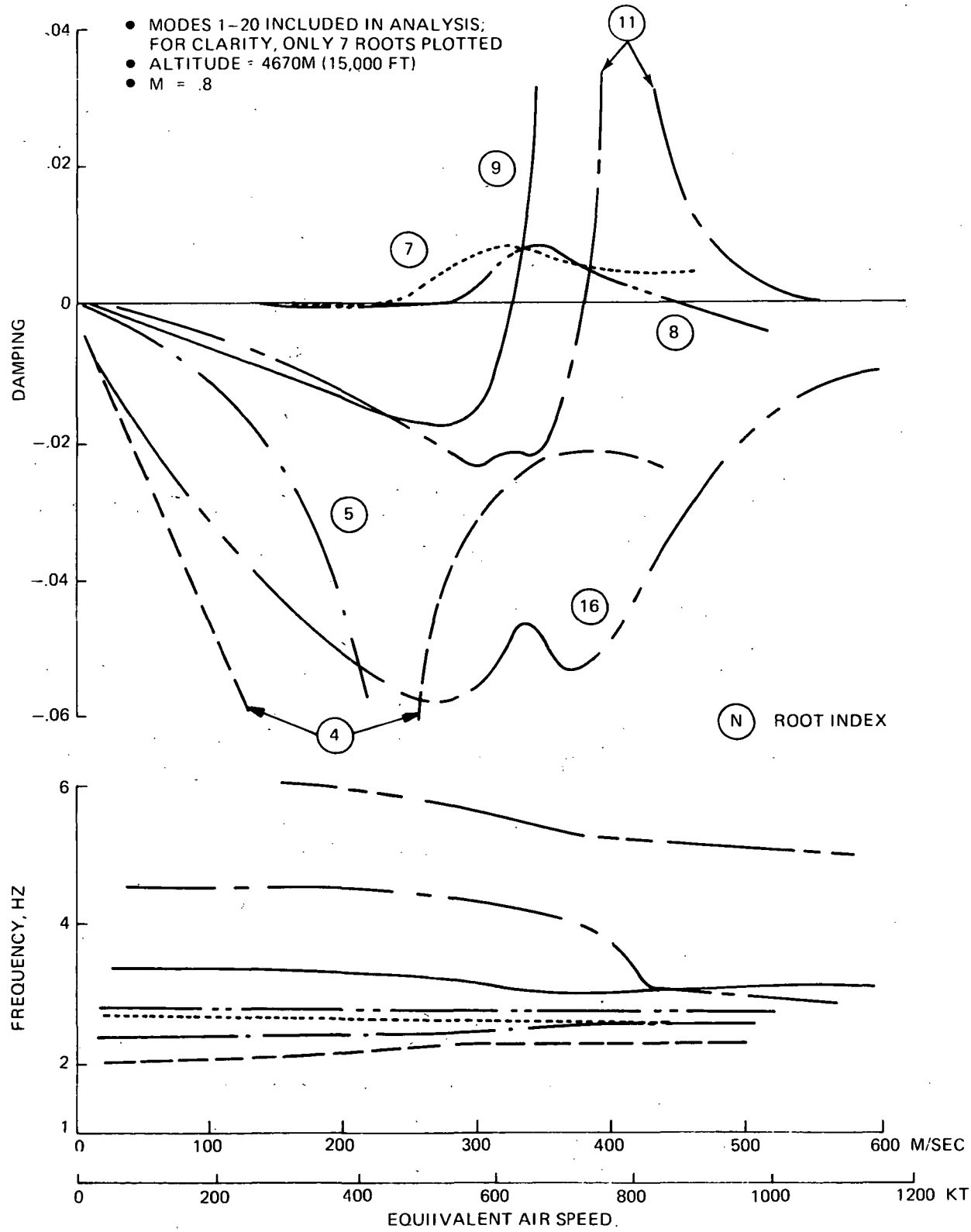

Fig. 15 V-g-f Plot for Symmetric Run 6A: Aerodynamics and Modes of the Complete Vehicle

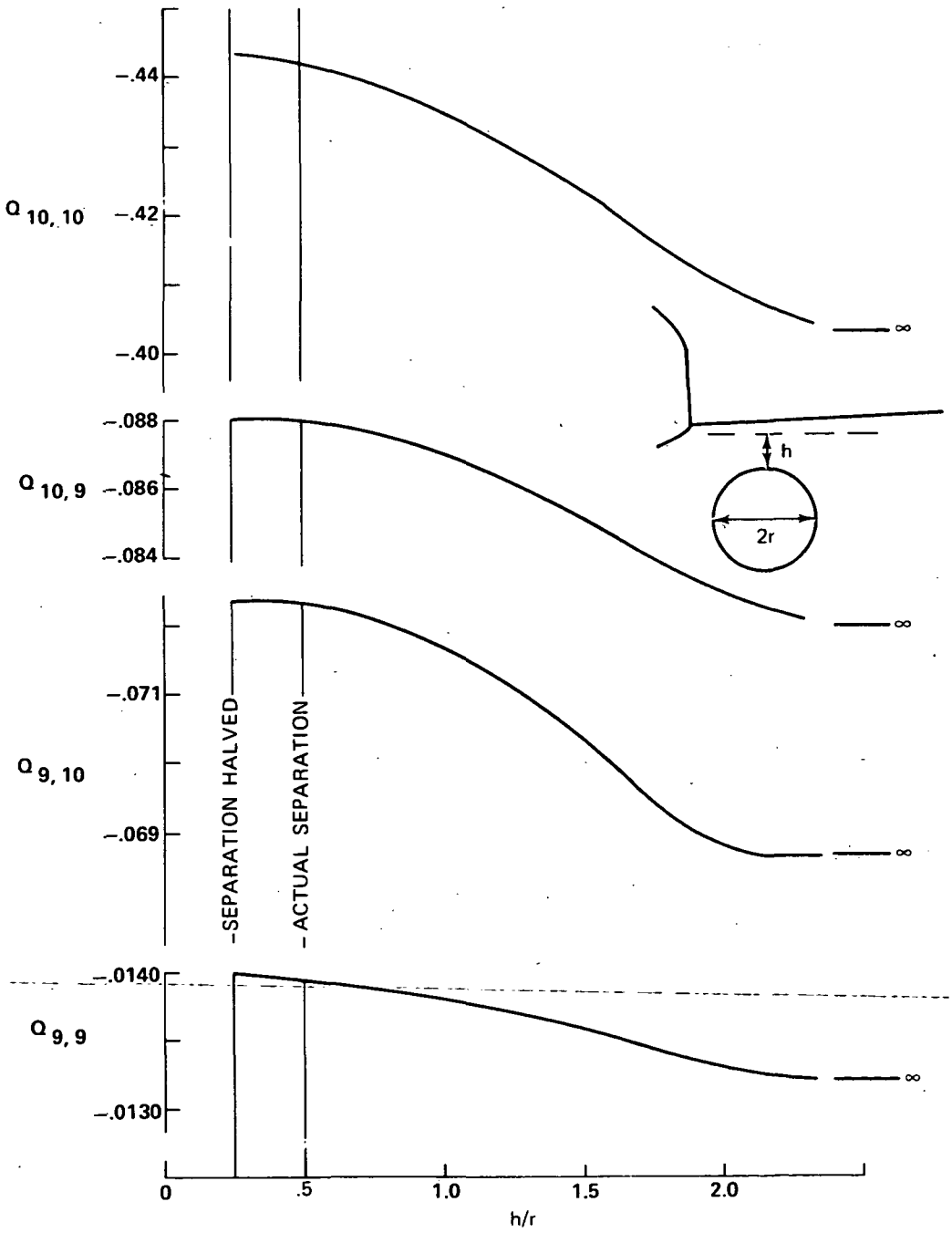

Fig. 16 Nondimensional, Real, Generalized, Aerodynamic Wing Forces as a Function of SRB Separation

NATIONAL AERONAUTICS AND SPACE ADMINISTRATION
WASHINGTON, D.C. 20546

OFFICIAL BUSINESS
PENALTY FOR PRIVATE USE $300

SPECIAL FOURTH-CLASS RATE
BOOK

POSTAGE AND FEES PAID
NATIONAL AERONAUTICS AND
SPACE ADMINISTRATION
451

U.S.MAIL

POSTMASTER: If Undeliverable (Section 158 Postal Manual) Do Not Return

"The aeronautical and space activities of the United States shall be conducted so as to contribute . . . to the expansion of human knowledge of phenomena in the atmosphere and space. The Administration shall provide for the widest practicable and appropriate dissemination of information concerning its activities and the results thereof."

—NATIONAL AERONAUTICS AND SPACE ACT OF 1958

NASA SCIENTIFIC AND TECHNICAL PUBLICATIONS

TECHNICAL REPORTS: Scientific and technical information considered important, complete, and a lasting contribution to existing knowledge.

TECHNICAL NOTES: Information less broad in scope but nevertheless of importance as a contribution to existing knowledge.

TECHNICAL MEMORANDUMS: Information receiving limited distribution because of preliminary data, security classification, or other reasons. Also includes conference proceedings with either limited or unlimited distribution.

CONTRACTOR REPORTS: Scientific and technical information generated under a NASA contract or grant and considered an important contribution to existing knowledge.

TECHNICAL TRANSLATIONS: Information published in a foreign language considered to merit NASA distribution in English.

SPECIAL PUBLICATIONS: Information derived from or of value to NASA activities. Publications include final reports of major projects, monographs, data compilations, handbooks, sourcebooks, and special bibliographies.

TECHNOLOGY UTILIZATION PUBLICATIONS: Information on technology used by NASA that may be of particular interest in commercial and other non-aerospace applications. Publications include Tech Briefs, Technology Utilization Reports and Technology Surveys.

Details on the availability of these publications may be obtained from:

SCIENTIFIC AND TECHNICAL INFORMATION OFFICE

NATIONAL AERONAUTICS AND SPACE ADMINISTRATION

Washington, D.C. 20546